Cell Metabolism

Article

Gut substrate trap of D-lactate from microbiota improves blood glucose and fatty liver disease in obese mice

Graphical abstract

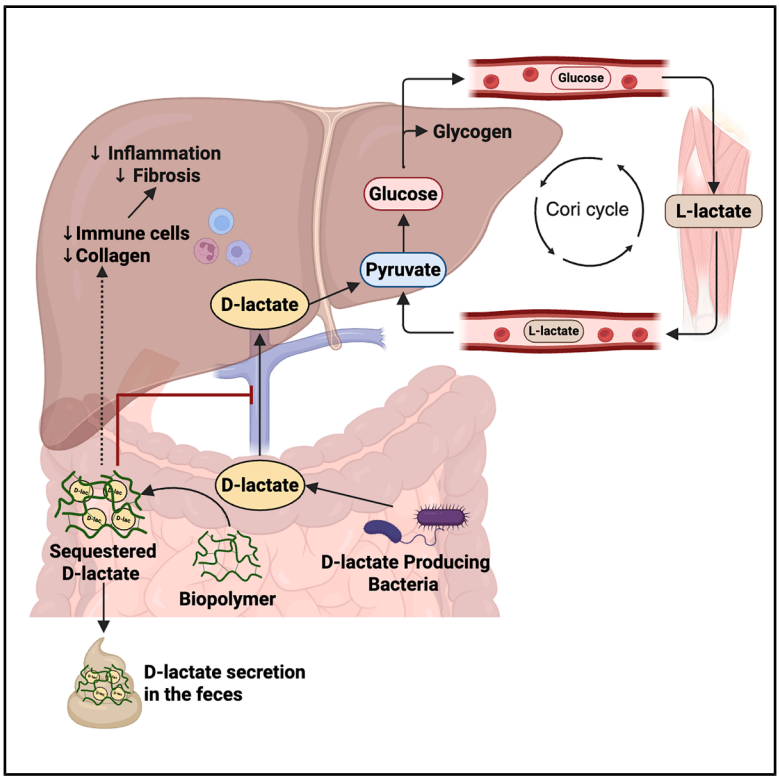

Highlights

- Blood D-lactate is higher during obesity in mice and humans
- Gut microbiota is the main source of D-lactate in mice
- Microbiota-derived D-lactate raises host blood glucose
- A gut substrate trap of D-lactate lowers blood glucose and MAFLD in obese mice

Authors

Han Fang, Fernando F. Anhê, Dana Kukje Zada, ..., André Tchernof, André Marette, Jonathan D. Schertzer

Correspondence

schertze@mcmaster.ca

In brief

D-lactate from the gut microbiota influences blood glucose and fatty liver disease. Trapping D-lactate in the gut improves blood glucose and lowers liver inflammation and fibrosis during obesity.

Fang et al., 2025, Cell Metabolism *37*, 1–14
September 2, 2025
https://doi.org/10.1016/j.cmet.2025.07.001

CellPress

Cell Metabolism

CellPress
OPEN ACCESS

Article

Gut substrate trap of D-lactate from microbiota improves blood glucose and fatty liver disease in obese mice

Han Fang,[1,6] Fernando F. Anhê,[1,6] Dana Kukje Zada,[1] Nicole G. Barra,[1] Rodrigo Rodrigues e-Lacerda,[1] Breanne T. McAlpin,[1] Ryan Wylie,[2] Line Berthiaume,[3] Étienne Audet-Walsh,[3] Conor O'Dwyer,[4] Peyman Ghorbani,[4] Morgan D. Fullerton,[4] Claudia Gagnon,[5] André Tchernof,[5] André Marette,[5] and Jonathan D. Schertzer[1,7,*]

[1]Department of Biochemistry and Biomedical Sciences, Farncombe Family Digestive Health Research Institute, and Centre for Metabolism, Obesity and Diabetes Research, McMaster University, Hamilton, ON L8N 3Z5, Canada
[2]Department of Chemistry and Chemical Biology, School of Biomedical Engineering, McMaster University, Hamilton, ON L8S 4M1, Canada
[3]Department of Molecular Medicine, Université Laval, Endocrinology and Nephrology Division, CHU de Québec–Université Laval Research Center (CRCHUQ-UL), Cancer Research Center (CRC) of Université Laval, Quebec City, QC, Canada
[4]Department of Biochemistry, Microbiology and Immunology, Faculty of Medicine, Centre for Infection, Immunity and Inflammation, Centre for Catalysis Research and Innovation, Ottawa Institute of Systems Biology, University of Ottawa, Ottawa, ON, Canada
[5]Quebec Heart and Lung Institute Research Centre, Laval University, Quebec, QC G1V 4G5, Canada
[6]These authors contributed equally
[7]Lead contact
*Correspondence: schertze@mcmaster.ca
https://doi.org/10.1016/j.cmet.2025.07.001

SUMMARY

L-lactate participates in metabolism, including the Cori cycle, but less is known about D-lactate. We found that circulating D-lactate was higher in humans and mice with obesity. D-lactate increased hepatic glycogen, triglycerides, and blood glucose more than equimolar L-lactate in mice. Stable isotope analyses showed that D-lactate is metabolized in mice and in hepatocytes to pyruvate, TCA intermediates, lipids, and glucose. The gut microbiota is the main source of blood D-lactate. Colonization of mice with a bacterial strain that produced D-lactate elevated blood glucose more than an L-lactate producer. Oral delivery of a biocompatible polymer that traps gut D-lactate, forcing fecal excretion, lowered blood glucose and insulin resistance in obese mice in a polymer length- and dose-dependent manner. This D-lactate trap lowered hepatic inflammation and fibrosis in mice with metabolic dysfunction-associated fatty liver disease (MAFLD)/metabolic dysfunction-associated steatohepatitis (MASH). Therefore, microbial-derived D-lactate contributes to host glucose and lipid metabolism and can be trapped to improve metabolic disease during obesity.

INTRODUCTION

Obesity is the strongest risk factor for type 2 diabetes (T2D) and metabolic dysfunction-associated fatty liver disease (MAFLD). These interlinked diseases cause a high health and economic burden.[1,2] Obesity, T2D, and MAFLD are associated with changes in the intestinal microbiota, including alterations in bacterial taxonomy, function, and bacterial metabolites.[3–5] Gut bacteria can contribute to host energy balance and nutrient absorption and produce metabolites that are substrates for host metabolism.[6–9] The gut microbiota can regulate blood glucose solely via hepatic gluconeogenesis without altering energy expenditure.[10,11] Little is known about the identity of microbiota-derived molecules that contribute to hepatic gluconeogenesis and lipogenesis. Typically, the microbiota is considered a source of inflammatory ligands, but its ability to directly fuel metabolic processes involved in T2D and MAFLD progression to metabolic dysfunction-associated steatohepatitis (MASH) should be considered.

We hypothesized that microbial D-lactate influences liver metabolism. It was originally thought that mammals lacked D-lactate dehydrogenases (D-LDHs), and consequently, D-lactate was not well metabolized to pyruvate. It was incorrectly hypothesized that D-lactate had to be metabolized by D-α-hydroxy acid dehydrogenase, which is 5 times slower than LDHs.[12] However, mice and humans have D-LDHs.[13,14] It is textbook knowledge that L-lactate derived from skeletal muscle glycolysis fuels the liver to produce glucose in the Cori cycle.[15] Cori and Cori made this discovery using D-lactate extracted from bacteria and found that oral delivery or injection of D-lactate in rodents leads to glycogen deposition in the liver, whereas exogenous L-lactate delivery "hardly forms any liver glycogen."[15] Over 75% of infused D-lactate is metabolized in healthy men.[16] D-lactate and L-lactate enantiomers have similar chemical and physical properties, and monocarboxylate transporters (MCT1–8) can transport both D- and L-lactate.[12] MCT1 is a key transporter in the intestine and liver and has a higher

Please cite this article in press as: Fang et al., Gut substrate trap of D-lactate from microbiota improves blood glucose and fatty liver disease in obese mice, Cell Metabolism (2025), https://doi.org/10.1016/j.cmet.2025.07.001

K_m for D-lactate compared with L-lactate in both tissues.[12,14] The rates of gluconeogenesis and oxidation from L- and D-lactate are comparable in bovine kidney, heart, and liver tissue *in vitro*.[17] Despite evidence that D-lactate can be metabolized in mammals, its metabolic fate is unknown.

People with diabetes and rodent models of diabetes both have higher levels of blood and urine D-lactate.[18,19] It is often assumed that the increased methylglyoxal pathway flux is responsible for the doubling of blood D-lactate in T2D.[20] However, bacteria can also produce D-lactate, including gut commensals in the *Lactobacillus* genera. Serum D-lactate is also higher in MAFLD patients, and serum D-lactate is correlated with the severity of MAFLD.[21] D-lactate is more immunogenic compared with L-lactate.[22] As such, D-lactate activates hepatic Kupffer cells and promotes neutrophil recruitment to the liver during infection.[23,24] However, the role of D-lactate in inflammation during MAFLD is unknown.

Since the portal circulation connects the gut and liver, we hypothesized that gut microbiota-derived D-lactate participates in host metabolism related to hepatic control of blood glucose and liver fat. We found that D-lactate participates in host glucose and lipid metabolism and that a single strain of bacteria that produces more D-lactate can raise blood glucose in mice. We also hypothesized that sequestration and elimination of gut microbiota-derived D-lactate before it crosses the gut barrier using a substrate trap of D-lactate produced by bacteria in the lumen of the gut would lower blood glucose during obesity and lower a trigger for liver inflammation during MAFLD. We designed a new biocompatible D-lactate gut substrate trap and found that oral delivery of this polymer lowered blood glucose, markers of insulin resistance, and hepatic inflammation and fibrosis in obese mice.

RESULTS

Blood D-lactate is higher in obese mice and humans

We determined D-lactate concentration in a genetic mouse model of obesity with and without hyperglycemia using *ob/ob* mice that experience transient hyperglycemia around 10 weeks old and return to normoglycemia at 20 weeks old due to increased insulin secretion. We found that D-lactate levels were significantly higher in the portal and systemic serum of male *ob/ob* mice at both 10 and 20 weeks old compared with their age-matched wild-type (WT) controls, whereas L-lactate was not different (Figures 1A–1D and 1G–1J). The obesity-related increase in D-lactate was larger in portal blood compared with the systemic blood (i.e., 11.8-fold versus 3.6-fold increase in *ob/ob* mice). People with obesity had higher plasma D-lactate levels, but L-lactate was not different (Figures 1E and 1F). We confirmed that higher maximal enzymatic activity of L-lactate dehydrogenase (L-LDH) compared with D-LDH in the liver mirrored the higher concentrations of blood L-lactate versus D-lactate in mice (i.e., L-lactate and L-LDH are 30–50 times higher) (Figures S1H–S1K). Compared with WT mice, D-lactate was significantly higher in the cecum and feces of *ob/ob* mice (Figures 1K–1M). Antibiotic treatment significantly decreased D-lactate in the cecum and feces of *ob/ob* mice to a level that is similar to the WT mice (Figures 1K–1M). Antibiotics also lowered serum D-lactate and random-fed blood glucose in *ob/ob* mice (Figures 1O and 1Q). Cecum and fecal L-lactate levels were also decreased after antibiotics, but this decrease did not affect serum levels of L-lactate (Figures 1L, 1N, and 1P). These data show that microbial-derived D-lactate underpins increased blood D-lactate during obesity, whereas the contribution of microbial L-lactate to systemic L-lactate is negligible.

D-lactate promotes higher liver glycogen, triglycerides, and blood glucose compared with L-lactate

Specific pathogen-free (SPF) mice had higher hepatic glycogen and triglycerides versus germ-free mice in both the fasted and re-fed states (Figures 2A–2E). Mice injected with D-lactate had higher glycogen when fasted and re-fed and higher triglycerides when re-fed (Figures 2F–2J). Injection of sodium lactate causes stress,[25] and 4 g/kg injections increased blood levels (Figures S1A and S1B). Gavage of 1 g/kg did not alter systemic blood D-lactate but increased portal D-lactate levels within the first 20 min (Figures S1C and S1E). Systemic L-lactate levels were increased in both control and high-fat diet (HFD)-fed mice after gavage of 1 g/kg L-lactate (Figure S1D). After oral gavage of 1 g/kg of either L-lactate or D-lactate, HFD-fed mice had higher blood glucose compared with mice on a control diet (Figures 2K–2O). D-lactate ingestion caused higher blood glucose compared with L-lactate in obese HFD-fed mice but not in lean mice on a control diet (Figures 2P–2S). In lean germ-free mice, blood glucose was also not different after gavage of 1 g/kg of L- or D-lactate (Figures S1F and S1G). These data demonstrate that D-lactate fuels glycogen and triglyceride synthesis in the liver and raises higher blood glucose levels more than L-lactate in obese mice.

D-lactate participates in whole-body metabolism and contributes to the TCA cycle, gluconeogenesis, and lipogenesis in hepatocytes

We next showed that oral/gut D-lactate can be metabolized by the host. We gavaged germ-free and SPF mice with ^{13}C-labeled glucose, L-lactate, or D-lactate and measured ^{13}C-labeled CO_2 in the expired breath of conscious mice using a stable isotope gas analyzer (Figure 3A). Germ-free and SPF mice oxidized oral glucose, L-lactate, and D-lactate at a comparable rate (Figures 3B–3G). We then used ^{13}C-labeled lactulose, a synthetic non-absorbable sugar. We showed that a gut commensal (*Lactobacillus delbrueckii*) can metabolize ^{13}C-labeled lactulose to produce ^{13}C-labeled D-lactate (Figure 3H). Using ^{13}C-labeled lactulose as a substrate, ~60% of the produced D-lactate contained ^{13}C, whereas less than 2% of the L-lactate contained ^{13}C (Figure 3I). We then gavaged germ-free and SPF mice with ^{13}C-labeled lactulose and measured $^{13}CO_2$ in their breath (Figure 3J). In the SPF mice, the gut commensals were able to convert lactulose into D-lactate, which was eventually metabolized into CO_2, where the time course for holobiont metabolism was ~twice as long compared with oral glucose, L-lactate, or D-lactate (Figures 3K and 3L). Germ-free mice could not metabolize oral lactulose due to a lack of gut microbiota. These data suggest that microbial-derived D-lactate can be utilized by the host as a fuel source.

We injected mice with either [^{14}C] L-lactate or [^{14}C] D-lactate to compare L- and D-lactate uptake and storage in the liver of mice (Figure 3M). There was no difference between D- or L-lactate uptake into total liver extracts or the aqueous and lipid

Please cite this article in press as: Fang et al., Gut substrate trap of D-lactate from microbiota improves blood glucose and fatty liver disease in obese mice, Cell Metabolism (2025), https://doi.org/10.1016/j.cmet.2025.07.001

CellPress
OPEN ACCESS

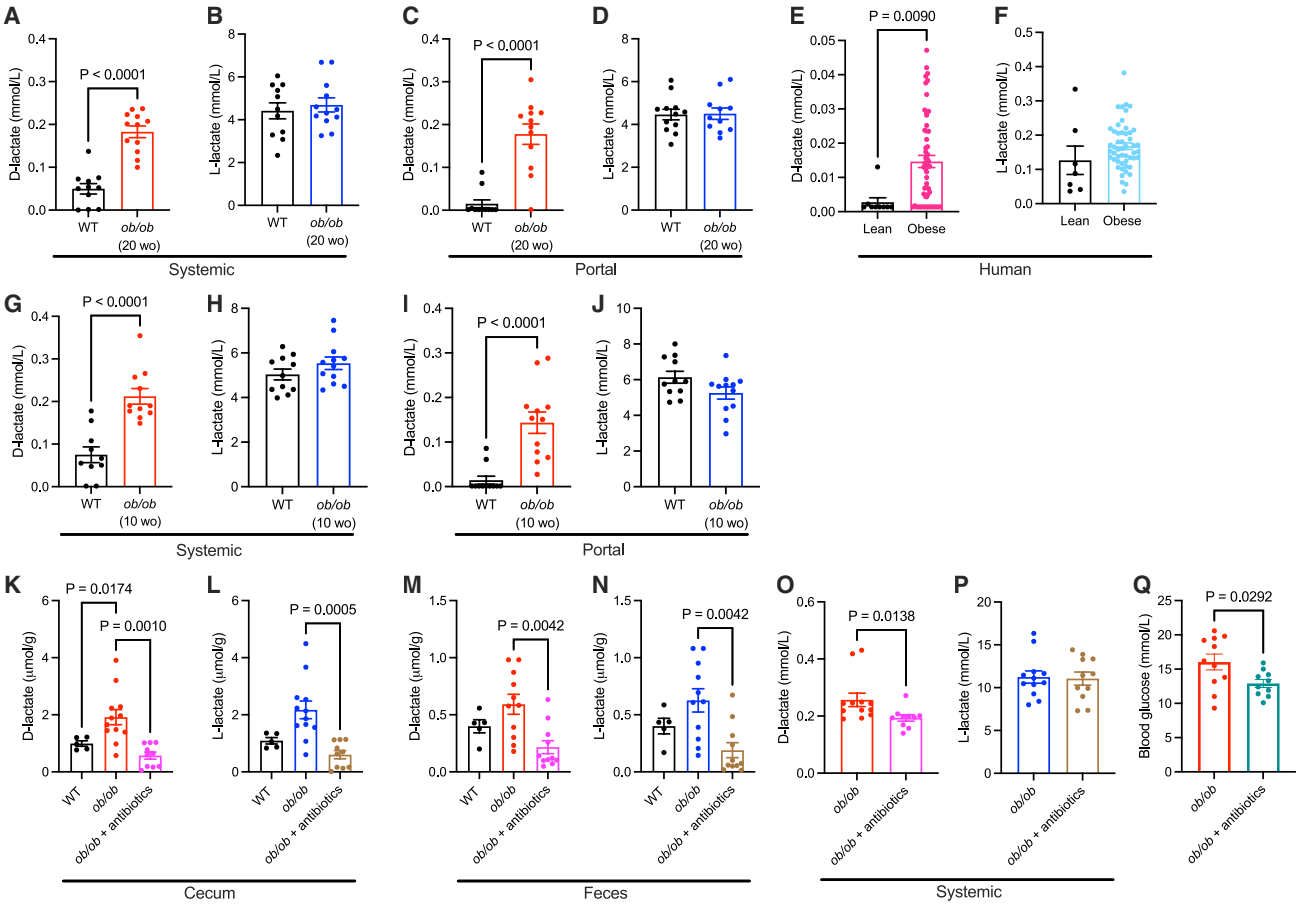

Figure 1. Blood D-lactate is higher in mice and humans with obesity

(A and B) (A) Systemic blood serum D-lactate and (B) L-lactate in 20-week-old WT and *ob/ob* mice.
(C and D) (C) Portal blood serum D-lactate and (D) L-lactate in 20-week-old WT and *ob/ob* mice.
(E and F) (E) Blood plasma D-lactate and (F) L-lactate in people that were non-obese and people with obesity.
(G and H) (G) Systemic blood serum D-lactate and (H) L-lactate in 10-week-old WT and *ob/ob* mice.
(I and J) (I) Portal blood serum D-lactate and (J) L-lactate in 10-week-old WT and *ob/ob* mice.
(K and L) (K) Cecal D-lactate and (L) L-lactate in 10-week-old WT, *ob/ob* mice, and *ob/ob* mice treated with antibiotics.
(M and N) (M) Fecal D-lactate and (N) L-lactate in 10-week-old WT, *ob/ob* mice, and *ob/ob* mice treated with antibiotics.
(O and P) (O) Systemic blood serum D-lactate and (P) L-lactate in 10-week-old *ob/ob* mice and *ob/ob* mice treated with antibiotics.
(Q) Blood glucose levels in 10-week-old *ob/ob* mice and *ob/ob* mice treated with antibiotics.
The numbers of independent biological replicates were (A–D) WT $n = 11$ and *ob/ob* $n = 11$–12; (E and F) non-obese $n = 7$–9 and obese $n = 51$–55; (G) WT $n = 10$ and *ob/ob* $n = 11$; (H–J) WT $n = 11$ and *ob/ob* $n = 12$; (K and L) WT $n = 5$, *ob/ob* $n = 12$, and *ob/ob* + antibiotics $n = 10$; (M and N) WT $n = 5$, *ob/ob* $n = 11$, and *ob/ob* + antibiotics $n = 11$; and (O–Q) *ob/ob* $n = 11$–12 and *ob/ob* + antibiotics $n = 10$–11. p values were calculated using unpaired t tests (A–J), Brown-Forsythe and Welch ANOVA (K), Kruskal-Wallis test (L–N), Mann-Whitney test (O), or Welch's t test (P and Q) and considered statistically significant at $p < 0.05$. Graphs depict mean ± SEM.

phases in the liver of mice (Figure 3N). We treated murine primary hepatocytes with [3-^{13}C] L-lactate or [3-^{13}C] D-lactate (Figure 3O). We found that 75%–80% of the L-lactate contained ^{13}C in hepatocytes (Figure 3P). In [3-^{13}C] L-lactate-treated primary hepatocytes, ~60% of pyruvate, 30% of glucose, 40%–60% of tricarboxylic acid cycle (TCA) intermediates, 2% of palmitic acid, 50% of aspartate, and 44% of glutamate contained ^{13}C (Figures 3Q–3V). Similarly, [3-^{13}C] D-lactate-treated primary hepatocytes had ~80% ^{13}C enrichment of D-lactate and ~35% of pyruvate, 15% of glucose, 20%–30% of TCA intermediates, and 1.5% of palmitic acid, 22% of aspartate, and 20% of glutamine contained ^{13}C (Figures 3W–3AC).

We showed that physiological levels of [3-^{13}C] D-lactate (0.4 mM) and [3-^{13}C] L-lactate (4 mM) can be metabolized by primary hepatocytes. About 50%–60% of the L- or D-lactate was labeled with ^{13}C (Figures S2A and S2G). We observed ^{13}C enrichment in pyruvate, glucose, TCA intermediates, aspartate, and glutamate in both [3-^{13}C] D-lactate- and [3-^{13}C] L-lactate-treated cells (Figures S2B–S2F and S2H–S2L). The level of enrichment is roughly 10 times higher in the L-lactate than in the D-lactate-treated cells. These data indicate that both D- and L-lactate are taken up by the liver and are metabolized in the TCA cycle, gluconeogenic and lipogenic pathways in hepatocytes.

Please cite this article in press as: Fang et al., Gut substrate trap of D-lactate from microbiota improves blood glucose and fatty liver disease in obese mice, Cell Metabolism (2025), https://doi.org/10.1016/j.cmet.2025.07.001

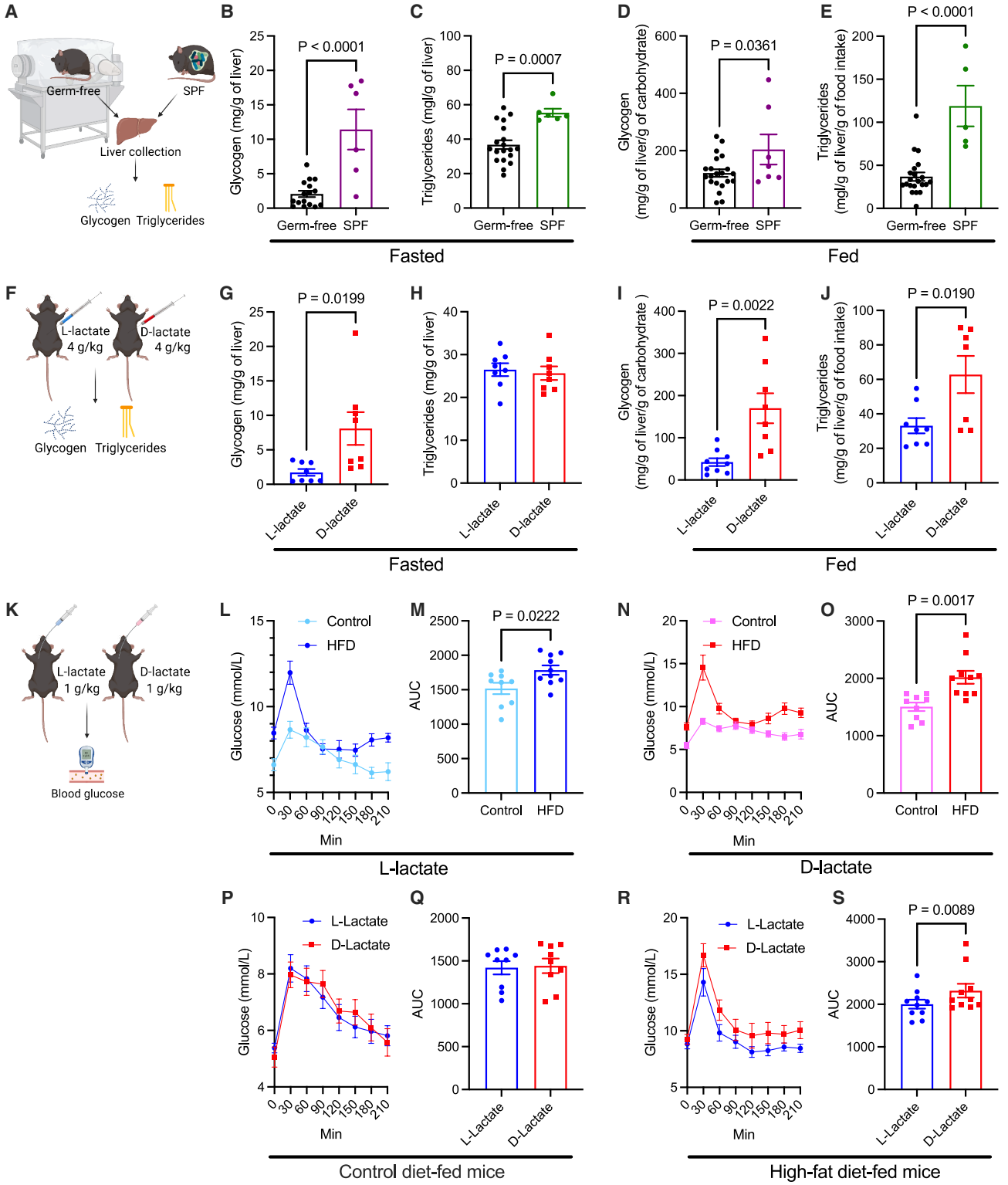

Figure 2. D-lactate promotes higher blood glucose, liver glycogen, and liver triglycerides compared with equimolar L-lactate

(A) Livers were collected from age-matched germ-free or SPF mice.

(B and C) (B) Liver glycogen and (C) triglyceride content in germ-free and SPF mice after 12 h of fasting.

(D and E) (D) Liver glycogen and (E) triglyceride content in germ-free and SPF mice after 12 h of fasting and 2 h of refeeding.

(F) Liver samples were collected from C57BL/6N mice receiving either 4 g/kg of L-lactate or D-lactate via intraperitoneal (i.p.) injection.

(G and H) (G) Liver glycogen and (H) triglyceride content in mice after 12 h fasting and 2 h after L-lactate or D-lactate injection.

(legend continued on next page)

Please cite this article in press as: Fang et al., Gut substrate trap of D-lactate from microbiota improves blood glucose and fatty liver disease in obese mice, Cell Metabolism (2025), https://doi.org/10.1016/j.cmet.2025.07.001

Microbial D-lactate increases host blood glucose

We show that gut microbiota are major contributors to blood D-lactate by comparing germ-free mice to mice that were born germ-free but then "conventionalized" through exposure to microbiota from SPF mice (Figure 4A). Age-matched conventionalized mice had higher levels of D-lactate in systemic blood compared with germ-free mice in both fasted and fed states, whereas L-lactate levels were similar (Figures 4B–4E).

We colonized germ-free mice with a strain of bacteria that produces either a high or low level of D-lactate (Figure 4F). *In vitro*, the D-lactate^{HIGH} strain, *Lactobacillus intestinalis* ASF360, produced 100 times more D-lactate than the D-lactate^{LOW} strain, *Lactobacillus reuteri* I49, which is consistent with previous literature.[24] The total lactate production (D-lactate + L-lactate) was similar between the two strains (Figure 4G). Germ-free mice colonized with D-lactate^{HIGH} versus D-lactate^{LOW}-producing bacteria had similar body weight and food intake (Figures 4H and 4I). Mice colonized with the D-lactate^{HIGH} had higher random-fed blood glucose 2–4 weeks after initial colonization. Mice were then recolonized at week 6, and mice recolonized with the D-lactate^{HIGH} had higher random-fed blood glucose for weeks 7 and 8 (Figure 4J). Fasting blood glucose was also higher in mice colonized with D-lactate^{HIGH} compared with D-lactate^{LOW} at both weeks 2 and 7 (Figure 4K). Serum and fecal D-lactate were higher in mice colonized with D-lactate^{HIGH} compared with D-lactate^{LOW} at week 2, and elevated serum D-lactate persisted at week 7 (Figures 4L and 4N). L-lactate was not different in the blood or feces (Figures 4M and 4O). These data demonstrate that microbial-derived D-lactate contributes to host blood glucose levels and that a single strain of bacteria that produces more D-lactate can elevate fasted and fed blood glucose in mice. It appears to take ~2 weeks after colonization with a D-lactate producer to increase blood glucose.

A substrate trap of gut microbial D-lactate lowers blood glucose and liver fat

We first aimed to provide proof-of-principle that a non-absorbable, biocompatible, gut luminal D-lactate trap can acutely decrease blood glucose and liver fat. It is known that certain polymers of D-lactide form a stereocomplex with L-lactate.[26] We hypothesized that certain polymers of L-lactate would capture D-lactate in the gut. Polymers of L- or D-lactate are biodegradable, non-toxic, and already used in resorbable medical devices such as sutures, implants, and drug delivery systems.[27] We found that a 24-unit poly(L-lactide) (PL24) could bind/capture D-lactate in semi-permeable dialysis chambers and then performed an acute test in lean mice and compared oral delivery of a 24-unit poly(D-lactide) (PD24, an L-lactate trap), PL24 (D-lactate trap), and a 20-unit poly(D-L-lactide) (PDL20, a combined D- and L-lactate trap) (Figure 5A). As a control, PD24 did not affect blood glucose, but PL24 and PDL20 both lowered blood glucose 4 h after oral delivery (Figure 5B). We found that microbial D-lactate is required for the blood glucose-lowering effects of PL24. Compared with PD24, blood glucose remained unchanged 4 h after PL24 treatment in both germ-free mice and germ-free mice colonized with D-lactate^{LOW} bacteria (Figures 5C and 5D). Since D-lactate fueled liver triglyceride synthesis, we fed obese mice HFD containing 10% PL24 for 1 day (Figure 5E). Liver triglyceride content was reduced in mice that received HFD containing 10% PL24 compared with HFD only (Figure 5F).

We tested if intervening with dietary PL24 could improve blood glucose in mice with preexisting obesity using mice fed an HFD for 23 weeks and then switched to a diet with or without 10% PL24 for 7 additional weeks (Figure 5G). In both fasted and fed conditions, serum D-lactate levels were lower in mice that consumed PL24, whereas serum L-lactate was unchanged (Figures 5H–5K). 24-h fecal output of D-lactate was higher in mice that consumed PL24, whereas L-lactate was unchanged (Figures 5L and 5M). Fasting blood glucose, fasting insulin, and the HOMA-IR index were all lower in mice that consumed PL24 (Figures 5N–5P). PL24 did not alter body mass or caloric intake (Figures 5Q and 5R). These data show that dietary PL24 traps gut D-lactate (but not L-lactate), which increases fecal excretion of D-lactate, thereby lowering blood D-lactate, blood glucose, and blood insulin in obese mice.

We tested polymer length using 10% dietary PL10 (shortest polymer), PL38, and PL65 (longest polymer) in HFD-fed obese mice (Figure S3A). HOMA-IR and fasting blood glucose were lower in obese mice fed PL38 and PL65 compared with HFD alone (Figures S3B and S3C), but fasting insulin was not different (Figure S3D). Random-fed blood glucose was measured weekly, and the area under the curve (AUC) of random-fed blood glucose over 9 weeks was lower in PL38- and PL65-fed mice (Figures S3E and S3F). None of the polymers altered body weight or caloric intake (Figures S3G and S3H). We next tested the dose-response of dietary PL65 in mice with preexisting obesity during a shorter 4-week intervention with PL65 (Figure S3I). Fasting blood glucose was lower in mice that received 20% PL65 (Figure S3J). All doses of dietary PL65 (2%, 5%, 10%, and 20%) lowered blood glucose and AUC during a glucose tolerance test (Figures S3K and S3L). PL65 did not affect body mass, caloric intake, or serum TLR4 activity (i.e., metabolic endotoxemia) (Figures S3M–S3O). To further test the specificity of the polymer in the gut environment, we performed targeted metabolomics in the fecal samples collected from mice that ingested HFD (control) and HFD containing 20% PL65. There were no significant changes in branched-chain amino

(I and J) (I) Liver glycogen and (J) triglyceride content in mice after 12 h fasting and 2 h refeeding and 2 h after L-lactate or D-lactate injection.
(K) Blood glucose after oral gavage of 1 g/kg of L-lactate or D-lactate in either control or HFD-fed mice.
(L and M) (L) Glucose over time and (M) AUC in control or HFD-fed mice after L-lactate gavage.
(N and O) (N) Glucose over time and (O) AUC in control or HFD-fed mice after D-lactate gavage.
(P and Q) (P) Glucose over time and (Q) AUC in control diet-fed mice after L-lactate versus D-lactate gavage.
(R and S) (R) Glucose over time and (S) AUC in HFD-fed mice after L-lactate or D-lactate gavage.
The numbers of independent biological replicates tested were (B and C) germ-free n = 16–19 and SPF n = 6, (D and E) germ-free n = 21 and SPF n = 7, (G–J) L-lactate n = 8–9 and D-lactate n = 7–8, (L–O) control n = 9 and HFD n = 10, and (P–S) L-lactate n = 10 and D-lactate n = 10. p values were calculated using unpaired t tests (B–E, G–J, M, and O) and paired t test (Q and S) and considered statistically significant at $p < 0.05$. Graphs depict mean ± SEM.

Please cite this article in press as: Fang et al., Gut substrate trap of D-lactate from microbiota improves blood glucose and fatty liver disease in obese mice, Cell Metabolism (2025), https://doi.org/10.1016/j.cmet.2025.07.001

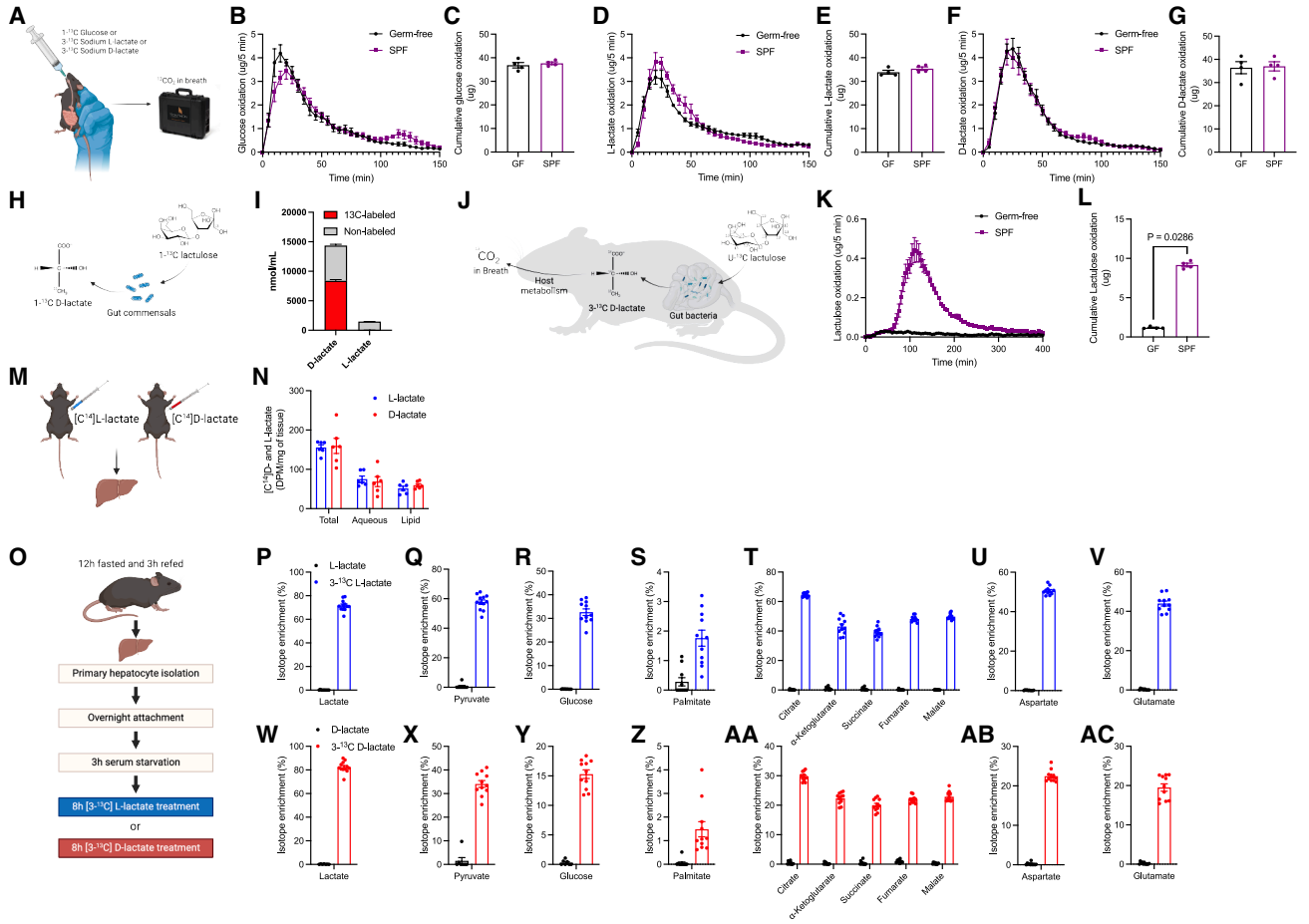

Figure 3. D-lactate participates in whole-body metabolism and the TCA cycle, gluconeogenesis, and lipogenesis in hepatocytes

(A) ^{13}C-labeled glucose, L-lactate, or D-lactate was gavaged in mice, and ^{13}C in the CO_2 from expired breath was measured using a stable isotope gas analyzer.
(B and C) (B) Glucose oxidation measured as μg of $^{13}CO_2$ every 5 min and (C) cumulative glucose oxidation.
(D and E) (D) L-lactate oxidation measured as μg of $^{13}CO_2$ every 5 min and (E) cumulative L-lactate oxidation.
(F and G) (F) D-lactate oxidation measured as μg of $^{13}CO_2$ every 5 min and (G) cumulative D-lactate oxidation.
(H) A gut commensal (*Lactobacillus delbruekii subsp. bulgaricus*) was cultured in de Man, Rogosa, and Sharpe (MRS) broth without dextrose and with 1-$^{13}C^{fru}$-lactulose to trace D-lactate production from lactulose.
(I) ^{13}C-labeled and non-labeled D- and L-lactate measured by liquid chromatography-mass spectrometry (LC-MS).
(J) Germ-free and SPF mice were gavaged U-^{13}C-lactulose, and $^{13}CO_2$ from their breath was measured using the stable isotope gas analyzer.
(K and L) (K) Lactulose oxidation measured as μg of $^{13}CO_2$ every 5 min and (L) Cumulative lactulose oxidation.
(M) C57BL/6N mice were injected intravenously (i.v.) with [C^{14}] L-lactate or [C^{14}] D-lactate, and livers were collected.
(N) [C^{14}] L- and D-lactate DPMs per mg of liver tissue in total homogenates, aqueous phase, and lipid phase extracted from livers.
(O) C57BL/6N mice were fasted for 12 h and re-fed for 3 h, then primary hepatocytes were isolated and incubated overnight. After 3 h of serum starvation, these primary hepatocytes were treated with either [3-^{13}C] L-lactate or [3-^{13}C] D-lactate for 8 h.
(P–V) ^{13}C isotopomer enrichment in (P) lactate, (Q) pyruvate, (R) glucose, (S) palmitate, (T) TCA cycle intermediates (citrate, α-ketoglutarate, succinate, fumarate, and malate), (U) aspartate, and (V) glutamate in hepatocytes treated with non-labeled L-lactate or [3-^{13}C] L-lactate.
(W–AC) ^{13}C isotopomer enrichment in (W) lactate, (X) pyruvate, (Y) glucose, (Z) palmitate, (AA) TCA cycle intermediates (citrate, α-ketoglutarate, succinate, fumarate, and malate), (AB) aspartate, and (AC) glutamate in hepatocytes treated with non-labeled D-lactate or [3-^{13}C] D-lactate.
The numbers of independent biological replicates tested were (B–G) germ-free and SPF $n = 4$, (I) D- and L-lactate $n = 3$, (K and L) germ-free and SPF $n = 4$, (N) L-lactate $n = 6$ and D-lactate $n = 6$, (P–V) L-lactate $n = 7$–11 and [3-^{13}C] L-lactate $n = 11$, and (W–AC) D-lactate $n = 8$–11 and [3-^{13}C] D-lactate $n = 11$–12, two biological replicates in primary hepatocyte isolation and six technical replicates in each isolation. *p* values were calculated using the Mann-Whitney test (C, E, G, and L). Graphs depict mean ± SEM. DPMs, disintegrations per minute.

acids, short-chain fatty acids, and bile acids in the feces of PL65-treated mice compared with control animals (Figures S4A–S4C). These data indicate that dietary ingestion of polymers of L-lactate can lower blood glucose during a glucose challenge during the fasted state in obese mice, which depends on polymer length and dose.

A gut substrate trap of D-lactate lowers hepatic inflammation and fibrosis in MAFLD/MASH

We tested if dietary PL65 can mitigate aspects of fatty liver disease using an established model of MAFLD progression to MASH in mice.[28] Mice were placed on either a control diet, MASH diet, or MASH diet with 20% of PL65 packed into the

Please cite this article in press as: Fang et al., Gut substrate trap of D-lactate from microbiota improves blood glucose and fatty liver disease in obese mice, Cell Metabolism (2025), https://doi.org/10.1016/j.cmet.2025.07.001

CellPress
OPEN ACCESS

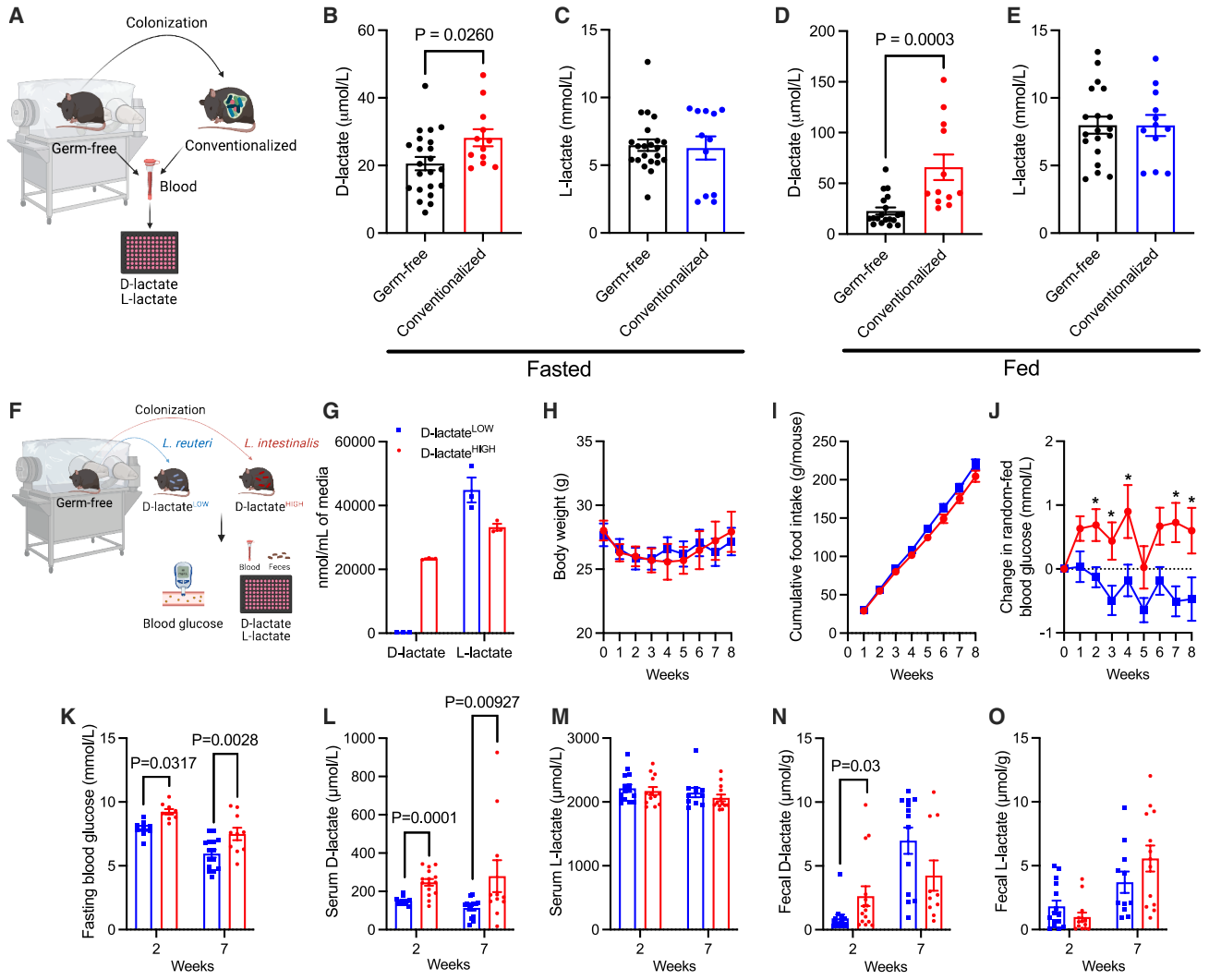

Figure 4. Microbiota is the main source of D-lactate, and microbial D-lactate increases host blood glucose

(A) Blood samples were collected from germ-free and conventionalized mice. Conventionalized mice were obtained by exposing previously germ-free mice to the microbiota from SPF mice for 23 weeks.

(B and C) (B) Systemic blood serum D-lactate and (C) L-lactate levels in germ-free and conventionalized mice after 24 h of fasting.

(D and E) (D) Systemic blood serum D-lactate and (E) L-lactate levels in random-fed germ-free and conventionalized mice.

(F) Germ-free mice were monocolonized with *Lactobacillus intestinalis* ASF360 (D-lactate^{HIGH}, produce high levels of D-lactate) or *Lactobacillus reuteri* 149 (D-lactate^{LOW}, produce low levels of D-lactate) upon export from germ-free cages (week 0) and then recolonized 6 weeks later.

(G) D-lactate and L-lactate production in bacterial culture media from D-lactate^{HIGH} and D-lactate^{LOW} strains.

(H–J) (H) Weekly body weight, (I) cumulative food intake, and (J) change in random-fed blood glucose in germ-free mice colonized with either D-lactate^{HIGH} or D-lactate^{LOW} strains.

(K) Fasting blood glucose at weeks 2 and 7.

(L and M) (L) Systemic blood serum D-lactate and (M) L-lactate at weeks 2 and 7.

(N and O) (N) Fecal D-lactate and (O) L-lactate at weeks 2 and 7.

The numbers of independent biological replicates tested were (B and C) germ-free $n = 22$ and conventionalized $n = 12$, (D and E) germ-free $n = 19$ and conventionalized $n = 12$, (G) D-lactate^{HIGH} $n = 3$ and D-lactate^{LOW} $n = 3$, (H–J) D-lactate^{HIGH} $n = 10$–16 and D-lactate^{LOW} $n = 14$, (K) D-lactate^{HIGH} $n = 9$–11 and D-lactate^{LOW} $n = 13$, and (L–O) D-lactate^{HIGH} $n = 11$–15 and D-lactate^{LOW} $n = 13$. p values were calculated using unpaired t tests (B–E) and two-way repeated measures ANOVA with Bonferroni's multiple comparison test (H–J) and Mann-Whitney U tests (G and K–O). p values were considered statistically significant at $p < 0.05$. Graphs depict mean ± SEM.

diet by weight (MASH + PL65) for 20 weeks. Dietary PL65 did not alter body weight or caloric intake (Figures S5A and S5B). The MASH diet increased liver mass, but the MASH + PL65 diet did not increase liver mass compared with the control diet (Figure S5C). The MASH diet increased HOMA-IR, blood glucose, and blood insulin (Figures 6A–6C). Dietary PL65 lowered HOMA-IR, blood glucose, and blood insulin compared with the MASH diet (Figures 6A–6C). Metabolic endotoxemia was also increased in the MASH group compared with controls; however, PL65 did not change metabolic endotoxemia in

Please cite this article in press as: Fang et al., Gut substrate trap of D-lactate from microbiota improves blood glucose and fatty liver disease in obese mice, Cell Metabolism (2025), https://doi.org/10.1016/j.cmet.2025.07.001

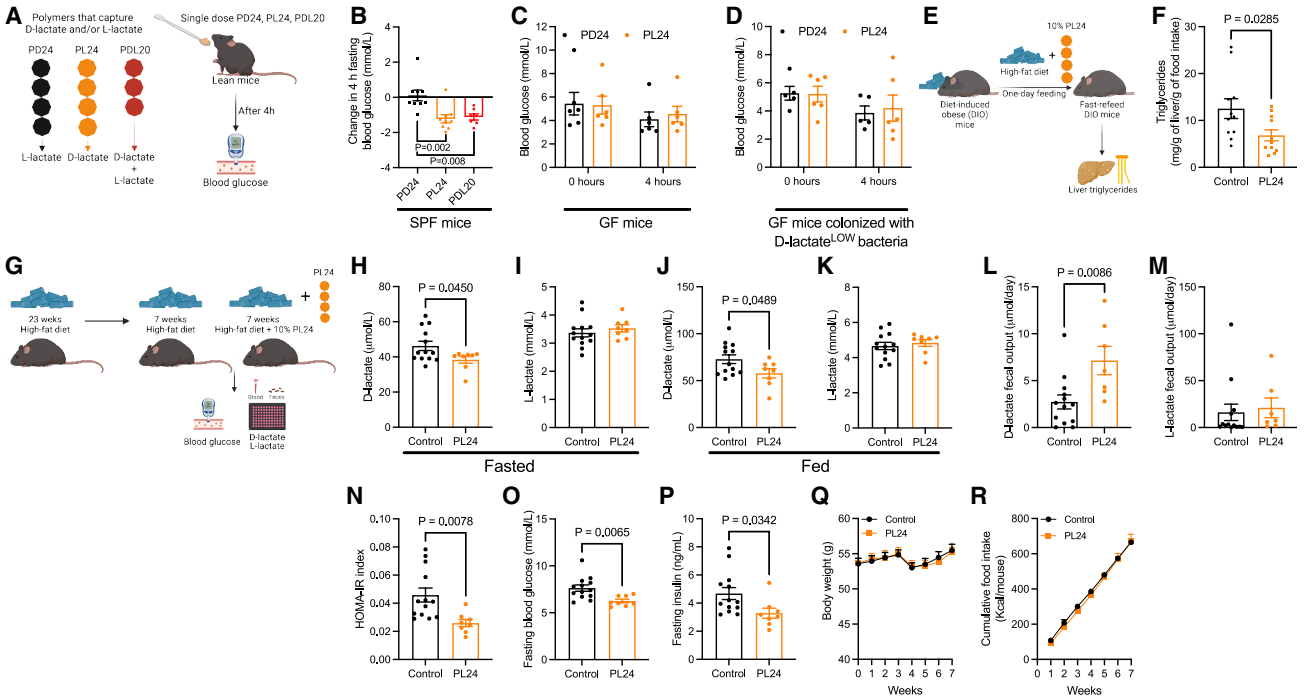

Figure 5. A gut substrate trap of microbial D-lactate trap lowers blood glucose and liver fat and improves insulin resistance in obese mice

(A) PD24 (poly-D-lactide), PL24 (poly-L-lactide), and PDL20 (poly-DL-lactide) can capture L-lactate and/or D-lactate.

(B) Change in fasting blood glucose 4 h after a single dose (100 mg) of PDL20, PD24, or P24 in lean mice.

(C and D) (C) Blood glucose before and 4 h after a single dose (100 mg) of PD24 or PL24 in germ-free mice and (D) germ-free mice colonized with D-lactate^{LOW} bacteria.

(E) Obese mice were on a 60% HFD for 29 weeks and then switched to 60% HFD + 10% PL24 for 1 day.

(F) Liver triglycerides in obese mice after 18 h of fasting and then re-fed for 2 h with 60% HFD or 1 day of 60% HFD + 10% PL24.

(G) Obese mice were on a 60% HFD for 23 weeks and then switched to 60% HFD with or without 10% PL24 in the diet for 7 weeks.

(H and I) (H) Serum D-lactate and (I) L-lactate in mice after 12 h fasting.

(J and K) (J) Serum D-lactate and (K) L-lactate in random-fed mice.

(L and M) (L) D-lactate and (M) L-lactate in the feces over 24 h.

(N–P) (N) Homeostatic Model Assessment of Insulin Resistance (HOMA-IR) index, (O) fasting blood glucose, and (P) fasting insulin after 12 h fasting.

(Q and R) (Q) Weekly body weight and (R) cumulative caloric intake for the 7 weeks after switching to 60% HFD with and without 10% PL24 in the diet. The numbers of independent biological replicates tested were (B) PDL20 $n = 7$, PD24 $n = 9$, and PL24 $n = 9$, (C and D) PD24 $n = 5$–6 and PL24 $n = 6$, (F) control $n = 11$ and PL24 $n = 11$, (H–Q) control $n = 13$ and PL24 $n = 7$–8, and (R) control $n = 3$ and PL24 $n = 3$, since food intake was monitored in each cage. p values were calculated using ordinary one-way ANOVA (B), two-way ANOVA (C and D), unpaired t test (F and H–P), and two-way repeated measures ANOVA with Bonferroni's multiple comparison test (Q and R). p values were considered statistically significant at $p < 0.05$. Graphs depict the mean ± SEM.

MASH-diet-fed mice (Figure S5E). The MASH diet increased the MASH activity score, which was calculated as the sum of steatosis, hepatocellular ballooning, and inflammation pathologist scores in hematoxylin and eosin (H&E)-stained liver sections in all five lobes (Figures 6D and 6E). Importantly, dietary PL65 lowered the MASH activity score (Figures 6D and 6E). The MASH diet increased liver steatosis and ballooning relative to the control diet, but the MASH + PL65 did not change liver steatosis and ballooning relative to the control diet (Figures 6F and 6G). Dietary PL65 lowered the inflammation score, which was lower in both the control and MASH + PL65-fed mice relative to the MASH diet-fed mice (Figure 6H). Individual pathological scoring was also conducted for each lobe of the liver (Figure S6). PL65 reduced inflammation in all lobes of the liver, which was the most consistent effect of a dietary gut substrate trap of D-lactate during MASH. The right medial lobe had the lowest inflammation, fibrosis, and steatosis, whereas the caudate lobe had the highest, and all the other lobes showed intermediate disease progression (Figure S6). The left lateral lobe was chosen for more detailed analyses since it is the largest liver lobe and has an intermediate level of disease progression. The control group had lower steatosis indicated by oil red O (ORO) area compared with both the MASH and MASH + PL65 groups (Figures 6I and 6J). MASH diet-fed mice had higher hepatic myeloperoxidase (MPO) and eosinophilic peroxidase (EPO) activity compared with the control mice (Figures 6K and 6L). Dietary PL65 lowered MPO and EPO activity compared with the MASH diet-fed mice (Figures 6K and 6L). Dietary PL65 also lowered the area of F4/80 staining in the liver, indicative of lower liver-resident macrophages (Figures 6M and 6N). These data show that PL65 lowers liver neutrophils, eosinophils, and macrophages during MASH.

Livers from MASH diet-fed mice had higher hydroxyproline content compared with controls, but MASH + PL65 did not have higher hydroxyproline content compared with controls (Figure S5D). Hepatic fibrosis was scored by a pathologist based on picrosirius red (PSR) staining (Figures 6O–6R). MASH diet-fed

Please cite this article in press as: Fang et al., Gut substrate trap of D-lactate from microbiota improves blood glucose and fatty liver disease in obese mice, Cell Metabolism (2025), https://doi.org/10.1016/j.cmet.2025.07.001

CellPress
OPEN ACCESS

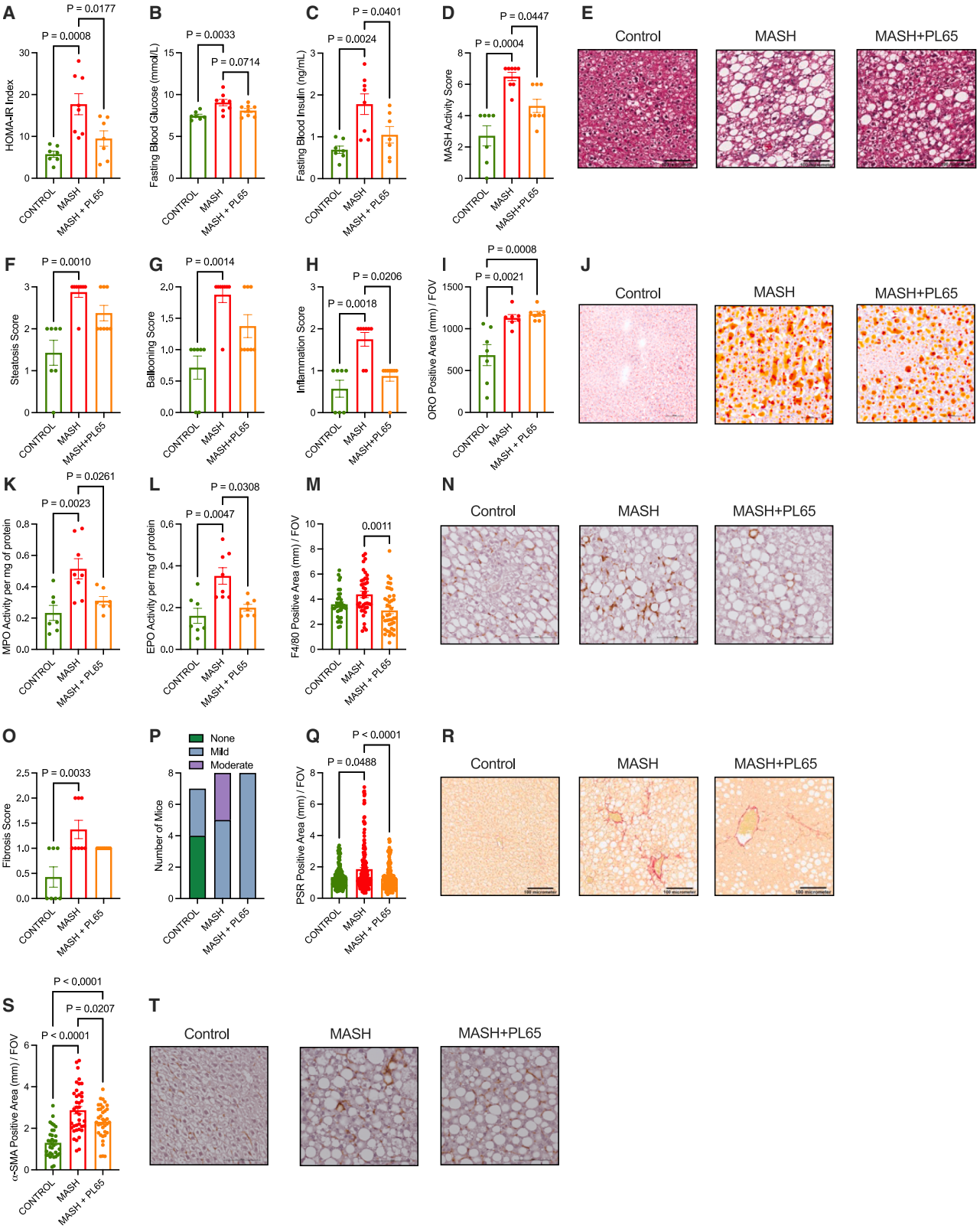

(legend on next page)

Please cite this article in press as: Fang et al., Gut substrate trap of D-lactate from microbiota improves blood glucose and fatty liver disease in obese mice, Cell Metabolism (2025), https://doi.org/10.1016/j.cmet.2025.07.001

mice had higher fibrosis compared with controls (Figure 6O). MASH + PL65-fed mice did not have higher fibrosis compared with controls (Figure 6O). Moderate zone 3 hepatic fibrosis was only seen in the MASH group but not in the controls or MASH + PL65-fed mice (Figure 6P). The PSR-positive area was quantified in all the liver lobes of each liver, and dietary PL65 lowered the area of PSR compared with the MASH diet-fed mice (Figures 6Q and 6R). The MASH group had a higher area of α-smooth muscle actin (SMA) compared with controls, and dietary PL65 lowered the area of α-SMA compared with the MASH diet-fed mice (Figures 6S and 6T). These results show that dietary PL65, a gut substrate trap of D-lactate, lowered blood glucose and insulin, lowered hepatic inflammation, and lowered hepatic fibrosis in obese mice.

DISCUSSION

The source of D-lactate and its role in energy metabolism and metabolic disease are poorly understood. We found that blood D-lactate is higher in obese mice and people with obesity and that gut microbiota is the main source of elevated D-lactate during obesity. D-lactate is rapidly metabolized in humans since after injection blood D-lactate levels peak by 5 min and return to basal levels within 30 min with no detectable D-lactate excretion in the urine.[29] The metabolic fate of D-lactate is unclear, but D-lactate may be a more efficient substrate for liver mitochondrial respiration compared with other tissues.[30,31] We investigated if D-lactate can be used as a substrate for gluconeogenesis, glycogen synthesis, and lipogenesis and directly compared equimolar D-lactate and L-lactate. We found higher liver glycogen content in mice that received D-lactate injection compared with L-lactate-injected mice under fasted and fed conditions. D-lactate was also described as "more efficient" for liver glycogen formation in rats in the Cori cycle.[15] We discovered that oral D-lactate promoted higher blood glucose compared with equimolar L-lactate in obese mice but not lean mice. It is not yet clear how obesity or an obesogenic diet alters the metabolism of D-lactate.

Estimations based on our data from mouse models suggest that D-lactate influences blood glucose through additional mechanisms beyond direct substrate supply. Multiple experiments showed that a change in blood D-lactate by 10–100 μmol/L corresponded with a ~1 mmol/L change in blood glucose. In addition, other glucoregulatory variables, such as blood insulin levels and liver inflammation, were altered by this magnitude of change in blood D-lactate. Therefore, the totality of the evidence to date supports the concept that the importance of D-lactate in altering host metabolism and/or blood glucose may not be as a quantitative fuel.

The reasons for potential differences in tissue-specific metabolism of L-lactate versus D-lactate are also not yet clear. D- and L-lactate are absorbed at the same rate by the intestine.[15] Beyond substrate availability of millimolar L-lactate versus micromolar D-lactate, L-lactate is used in the brain, muscle, and adipose tissue, which all contain the lactate receptor G protein-coupled receptor 81 (GPR81).[32] One previous study showed that oral gavage of D-lactate activates brown adipose tissue via GPR81 and alleviates metabolic dysfunction in diet-induced obese mice.[33] However, the D-lactate dose used in this previous study is much lower than the half maximal effective concentration (EC50) of D-lactate for GPR81 (20 mM),[34] and mice were not housed at thermoneutrality to study energy balance, which makes the results from this previous study hard to interpret.

D-lactate produced by gut microbiota is positioned to travel in the portal circulation and influence liver metabolism. We provided proof-of-principle evidence showing that colonization of mice with bacteria that produce higher D-lactate equates to higher blood glucose. Importantly, these experiments use a bacterial strain that was a fast producer of high D-lactate versus a strain of bacteria that produced L-lactate. Despite each strain of bacteria producing a similar total lactate load, the mice colonized with a

Figure 6. A gut D-lactate trap lowers hepatic inflammation and fibrosis in MALFD/MASH

(A–C) (A) HOMA-IR, (B) blood glucose, and (C) blood insulin after a 4-h fast.
(D) MASH activity score was calculated by a pathologist blinded to the experimental conditions based on the MASH clinical research network scoring system using all five lobes of the liver.
(E) Representative H&E images at 40× magnification.
(F–H) (F) Steatosis score, (G) ballooning score, and (H) inflammation score based on the MASH clinical research network scoring system using H&E-stained sections in all lobes of the liver.
(I) ORO-positive area in millimeters per field of view in the left lateral lobe at 20× magnification.
(J) Representative ORO images at 10× magnification.
(K) MPO enzymatic activity in the left lateral lobe of the liver.
(L) EPO enzymatic activity in the left lateral lobe of the liver was measured.
(M) F4/80 positive area in millimeters per field of view in the left lateral lobe at 20× magnification, and each point on the graph represents one image analyzed.
(N) Representative F4/80 images at 20× magnification.
(O) Fibrosis score based on the MASH clinical research network scoring system using PSR-stained sections in all lobes of the liver. A fibrosis score of 0 represents a score of 0 (no fibrosis), a score of 1 on the graphs represents a score of 1A (mild zone 3 perisinusoidal fibrosis), and a score of 2 represents a score of 1B (moderate zone 3 perisinusoidal fibrosis) using the MASH clinical research network scoring system.
(P) Breakdown of the number of mice assigned to each fibrosis score within each group.
(Q) PSR-positive area in millimeters per field of view in all lobes of the liver at 20× magnification, and each point on the graph represents one image analyzed.
(R) Representative PSR images at 40× magnification.
(S) α-SMA positive area in millimeters per field of view in the left lateral lobe at 20× magnification, and each point on the graph represents one image analyzed.
(T) α-SMA representative images at 20× magnification. The numbers of independent biological replicates tested were (A, C, K, and L) control $n = 7$, MASH $n = 8$, MASH + PL65 $n = 7$. (B, D–J, and O–S) Control $n = 7$, MASH $n = 8$, MASH + PL65 $n = 8$. (M) Control $n = 7$, MASH $n = 7$, MASH + PL65 $n = 7$. p values were calculated using ordinary one-way ANOVA (A–C, K, M, and Q) and Kruskal-Wallis test (F–I, L, O, and S). p values were considered statistically significant at $p < 0.05$. Graphs are mean ± SEM.

Please cite this article in press as: Fang et al., Gut substrate trap of D-lactate from microbiota improves blood glucose and fatty liver disease in obese mice, Cell Metabolism (2025), https://doi.org/10.1016/j.cmet.2025.07.001

D-lactate producer had higher blood glucose. These data suggest that gut microbiota-derived D-lactate is preferentially absorbed, transported, and/or metabolized into host blood glucose compared with microbial L-lactate. We found that D-lactate could be metabolized by hepatocytes *in vitro*, but a higher percentage of L-lactate was incorporated into glycogen, TCA intermediates, and even glucose. These data strongly suggest that *in vivo* transport or tissue communication signals dictate the fate of gut-derived D-lactate versus L-lactate. The role of D-lactate in immunometabolism and endocrine control of metabolism should also be considered. D-lactate can impact host immunity.[6] Gut microbiota-derived D-lactate improves immune defense against bacterial infection.[23,24] Commensal bacterial-derived D-lactate traverses the gut into the portal circulation, recruits neutrophils to the liver, and programs liver-resident Kupffer cells to promote immune defense (i.e., high inflammation) against systemic bacterial infections.

We aimed to sequester D-lactate derived from gut microbiota. We found that polymers of L-lactate bound D-lactate. This D-lactate trap was attractive because polymers of L-lactate, commonly referred to as polylactic acid (PLA), are biodegradable polymers already used in medical devices and drug delivery systems with good safety profiles. Given the isomeric relationship between D-lactate and L-lactate, it was known that a polymer of L-lactate decreases the free D-lactate concentration *in vitro* by forming a stereocomplex with D-lactate.[26] We found that oral delivery of specific poly-L-lactides, the cyclic ester formed by two lactic acid molecules, can force the excretion of gut D-lactate, thereby lowering blood D-lactate and blood glucose. We also found that specific poly-L-lactides could lower liver fat in obese mice acutely, which, along with the potentially immunogenic properties of microbial D-lactate in the liver, prompted us to test if poly-L-lactides could mitigate features of MAFLD or MASH.

We found that dietary supplementation with a poly-L-lactide (PL65) polymer as a gut D-lactate trap improved inflammation and fibrosis in a mouse model of MAFLD/MASH. The D-lactate trap did not alter liver fat content, which is consistent with a small contribution of D-lactate to lipogenesis (~2%) in primary mouse hepatocytes. The reduced liver fibrosis was confirmed by a pathologist and lower α-SMA, and this effect of PL65 may be linked to lower liver inflammation. Oral PL65 had the most consistent and profound effect on lowering inflammation, which occurred in all lobes of the liver. D-lactate promotes neutrophil infiltration to the liver by priming hepatic endothelial cells.[23] Neutrophil accumulation and release of MPO and neutrophil elastase in the liver is a key feature of MASH progression.[35] We show that PL65 lowers liver MPO and EPO, which is consistent with studies that show that depletion of neutrophils or lowering neutrophil effector molecules lowers MASH progression in mice.[36,37]

We showed that oral PL65 lowered a marker of liver macrophages. Bacterial-derived D-lactate can activate liver-resident macrophages (i.e., Kupffer cells).[24] Similar to neutrophils, Kupffer cells contribute to MASH progression.[21,38,39] Future research should determine how D-lactate alters liver immune responses in MAFLD and MASH.

In summary, we demonstrate that microbial-derived D-lactate influenced blood glucose. Trapping D-lactate in the gut with dietary, biocompatible polymers lowered blood glucose, lowered blood insulin, and improved glucose control in obese mice. A gut substrate trap of D-lactate also reduced hepatic inflammation and fibrosis in MASH. These findings expand our knowledge of the Nobel Prize-winning discovery of the Cori cycle. Microbial D-lactate represents a shunt in the Cori cycle where a microbial (non-host) source of D-lactate can be captured and sequestered in the gut, thereby providing potential therapeutics for obesity-induced dysglycemia and MAFLD/MASH.

Limitations of the study

One goal of this study was to compare equimolar D-lactate and L-lactate as proof-of-principle. Even though our experiments show that D-lactate had a higher potential to raise blood glucose and increase liver glycogen and hepatic fat compared with equimolar L-lactate, it is critical that L-lactate circulates in millimolar concentrations and blood D-lactate is generally 50- to 100-fold lower in mammals. We recognize the importance of L-lactate, which, based on the amount of substrate, exceeds the potential of D-lactate as a quantitative fuel for host metabolism. The difference between microbiota to generate a chronic load of D-lactate versus results obtained during a large oral bolus of D-lactate during a gavage should be carefully considered. We found differences in D-lactate versus L-lactate levels in the portal and systemic circulation after gavage and microbial colonization, but we cannot fully explain the divergent mechanism of action in L-lactate versus D-lactate metabolism.

Another limitation of this work is that we do not yet know how relatively small changes in D-lactate caused changes in blood glucose. We also do not know why hepatocytes in culture convert relatively less D-lactate to glucose, glycogen, and other intracellular intermediates, but D-lactate is an efficient substrate for metabolism *in vivo*. Future work should focus on other cell types and tissue communication of D-lactate metabolism integrated with substrate metabolism and excretion. Since our animal experiments were performed using male mice, exploring whether there is a sexual dimorphism in how D-lactate influences metabolic health is a future goal. Although we found that people with obesity have higher blood D-lactate, all other work was in cells or mice, which is a limitation of our study. Blood D-lactate levels are elevated in people with diabetes and positively correlated with MAFLD severity in humans.[18,19,21] Hence, an important future goal is to determine the human relevance of D-lactate metabolism and to consider the microbiota as a source of D-lactate that participates in metabolic disease. Future work should also aim to determine the amount of D-lactate that is generated by the host methylglyoxal pathway versus the microbiota in humans.

RESOURCE AVAILABILITY

Lead contact

Requests for resources will be fulfilled by the lead contact, Jonathan Schertzer (schertze@mcmaster.ca).

Materials availability

No unique materials or reagents were generated during this work.

Data and code availability

The datasets generated and/or analyzed are available in Data S1 and from the corresponding author upon reasonable request.

ACKNOWLEDGMENTS

We thank Dr. Kathy McCoy (University of Calgary) for sharing two strains of bacteria, *Lactobacillus intestinalis* ASF360 and *Lactobacillus reuteri* I49. H.F. was supported by a Farncombe Family Digestive Health Research Fellowship and a Center for Metabolism, Obesity, and Diabetes Research fellowship. F.F.A. was supported by a CIHR fellowship. D.K.Z. was supported by a Farncombe Family Digestive Health Research Studentship Award. J.D.S. holds a Canada Research Chair in Metabolic Inflammation. M.D.F. holds a Camille Villeneuve Research Chair in Cardiovascular Immunometabolism. This work was supported by a CIHR project grant (PJT-175054) to J.D.S. This work was supported by a John R. Evans Leaders equipment and infrastructure grant (#38622) to E.A.W. from the Canada Foundation for Innovation (CFI).

AUTHOR CONTRIBUTIONS

J.D.S., H.F., and F.F.A. designed experiments. Experiments were conducted by H.F., F.F.A., D.K.Z., N.G.B., R.R.e.-L., B.T.M., R.W., L.B., C.O., P.G., and C.G. A.T. and A.M. provided the human samples. Data analyzed by H.F., F.F.A., D.K.Z., É.A.-W., M.D.F., and J.D.S. Original draft written by H.F., F.F.A., D.K.Z., and J.D.S. Editing and reviewing by H.F., F.F.A., D.K.Z., É.A.-W., M.D.F., and J.D.S.

DECLARATION OF INTERESTS

H.F., F.F.A., and J.D.S. hold a patent related to compositions to modify intestinal nutrient absorption. A.T. receives funding from Johnson & Johnson, Medtronic, and BioTwin for research on bariatric surgery or obesity. A.T. acted as a consultant for Bausch Health, Eli Lilly, Novo Nordisk, and BioTwin.

STAR★METHODS

Detailed methods are provided in the online version of this paper and include the following:

- KEY RESOURCES TABLE
- EXPERIMENTAL MODEL AND SUBJECT DETAILS
  - Human samples
  - Animal models
- METHOD DETAILS
  - Biochemical analysis
  - D- and L-lactate levels during obesity
  - Circulating D- and L-lactate levels during lactate tolerance tests
  - D- and L-lactate in germ-free and conventionalized mice
  - Liver glycogen and triglyceride in germ-free and SPF mice after D- and L-lactate injection
  - Glucose and lactate tolerance tests
  - In vivo lactate injections
  - In vivo 13C tracing
  - Mouse primary hepatocytes
  - Mouse primary hepatocytes metabolite quantification
  - Colonization of Germ-free mice with D-lactate producers
  - Acute polylactide administration
  - Long-term feeding with PL24
  - Polylactide length and dose study
  - Fecal targeted metabolomics
  - PL65 in MAFLD/MASH
  - Metabolic endotoxemia measurement via HEK TLR4 reporter cell
  - MPO and EPO enzymatic activity assays
  - Hydroxyproline assay
  - Histology and immunohistochemistry
- QUANTIFICATION AND STATISTICAL ANALYSIS

SUPPLEMENTAL INFORMATION

Supplemental information can be found online at https://doi.org/10.1016/j.cmet.2025.07.001.

Received: December 12, 2024
Revised: May 9, 2025
Accepted: July 1, 2025

REFERENCES

1. Tran, B.X., Nair, A.V., Kuhle, S., Ohinmaa, A., and Veugelers, P.J. (2013). Cost analyses of obesity in Canada: scope, quality, and implications. Cost Eff. Resour. Alloc. *11*, 3. https://doi.org/10.1186/1478-7547-11-3.
2. Bilandzic, A., and Rosella, L. (2017). The cost of diabetes in Canada over 10 years: applying attributable health care costs to a diabetes incidence prediction model. Health Promot. Chronic Dis. Prev. Can. *37*, 49–53. https://doi.org/10.24095/hpcdp.37.2.03.
3. Loomba, R., Seguritan, V., Li, W., Long, T., Klitgord, N., Bhatt, A., Dulai, P. S., Caussy, C., Bettencourt, R., Highlander, S.K., et al. (2017). Gut Microbiome-Based Metagenomic Signature for Non-invasive Detection of Advanced Fibrosis in Human Nonalcoholic Fatty Liver Disease. Cell Metab. *25*, 1054–1062.e5. https://doi.org/10.1016/j.cmet.2017.04.001.
4. Tremaroli, V., and Bäckhed, F. (2012). Functional interactions between the gut microbiota and host metabolism. Nature *489*, 242–249. https://doi.org/10.1038/nature11552.
5. Pedersen, H.K., Gudmundsdottir, V., Nielsen, H.B., Hyotylainen, T., Nielsen, T., Jensen, B.A.H., Forslund, K., Hildebrand, F., Prifti, E., Falony, G., et al. (2016). Human gut microbes impact host serum metabolome and insulin sensitivity. Nature *535*, 376–381. https://doi.org/10.1038/nature18646.
6. Fang, H., Rodrigues e-Lacerda, R., Barra, N.G., Kukje Zada, D., Robin, N., Mehra, A., and Schertzer, J.D. (2024). Postbiotic Impact on Host Metabolism and Immunity Provides Therapeutic Potential in Metabolic Disease. Endocrine Reviews, bnae025. https://doi.org/10.1210/endrev/bnae025.
7. Anhê, F.F., Zlitni, S., Zhang, S.-Y., Choi, B.S.-Y., Chen, C.Y., Foley, K.P., Barra, N.G., Surette, M.G., Biertho, L., Richard, D., et al. (2023). Human gut microbiota after bariatric surgery alters intestinal morphology and glucose absorption in mice independently of obesity. Gut *72*, 460–471. https://doi.org/10.1136/gutjnl-2022-328185.
8. Bäckhed, F., Manchester, J.K., Semenkovich, C.F., and Gordon, J.I. (2007). Mechanisms underlying the resistance to diet-induced obesity in germ-free mice. Proc. Natl. Acad. Sci. USA *104*, 979–984. https://doi.org/10.1073/pnas.0605374104.
9. Bäckhed, F., Ding, H., Wang, T., Hooper, L.V., Koh, G.Y., Nagy, A., Semenkovich, C.F., and Gordon, J.I. (2004). The gut microbiota as an environmental factor that regulates fat storage. Proc. Natl. Acad. Sci. USA *101*, 15718–15723. https://doi.org/10.1073/pnas.0407076101.
10. Krisko, T.I., Nicholls, H.T., Bare, C.J., Holman, C.D., Putzel, G.G., Jansen, R.S., Sun, N., Rhee, K.Y., Banks, A.S., and Cohen, D.E. (2020). Dissociation of Adaptive Thermogenesis from Glucose Homeostasis in Microbiome-Deficient Mice. Cell Metab. *31*, 592–604.e9. https://doi.org/10.1016/j.cmet.2020.01.012.
11. Jastroch, M., Ussar, S., and Keipert, S. (2020). Gut Microbes Controlling Blood Sugar: No Fire Required! Cell Metab. *31*, 443–444. https://doi.org/10.1016/j.cmet.2020.02.007.
12. Ewaschuk, J.B., Naylor, J.M., and Zello, G.A. (2005). D-Lactate in Human and Ruminant Metabolism. J. Nutr. *135*, 1619–1625. https://doi.org/10.1093/jn/135.7.1619.
13. Flick, M.J., and Konieczny, S.F. (2002). Identification of putative mammalian D-lactate dehydrogenase enzymes. Biochem. Biophys. Res. Commun. *295*, 910–916. https://doi.org/10.1016/s0006-291x(02)00768-4.
14. De Bari, L., Atlante, A., Guaragnella, N., Principato, G., and Passarella, S. (2002). d-Lactate transport and metabolism in rat liver mitochondria. Biochem. J. *365*, 391–403. https://doi.org/10.1042/BJ20020139.
15. Cori, C.F., and Cori, G.T. (1929). GLYCOGEN FORMATION IN THE LIVER FROM d- AND l-LACTIC ACID. J. Biol. Chem. *81*, 389–403. https://doi.org/10.1016/S0021-9258(18)83822-4.

16. Oh, M.S., Uribarri, J., Alveranga, D., Lazar, I., Bazilinski, N., and Carroll, H. J. (1985). Metabolic utilization and renal handling of d-lactate in men. Metabolism *34*, 621–625. https://doi.org/10.1016/0026-0495(85)90088-5.

17. Harmon, D.L., Britton, R.A., and Prior, R.L. (1984). In vitro rates of oxidation and gluconeogenesis from L(+)- and D(-)lactate in bovine tissues. Comp. Biochem. Physiol. B *77*, 365–368. https://doi.org/10.1016/0305-0491(84)90344-4.

18. Talasniemi, J.P., Pennanen, S., Savolainen, H., Niskanen, L., and Liesivuori, J. (2008). Analytical investigation: assay of D-lactate in diabetic plasma and urine. Clin. Biochem. *41*, 1099–1103. https://doi.org/10.1016/j.clinbiochem.2008.06.011.

19. Lin, M.-H., Chen, H.-Y., Liao, T.-H., Huang, T.-C., Chen, C.-M., and Lee, J.-A. (2011). Determination of time-dependent accumulation of D-lactate in the streptozotocin-induced diabetic rat kidney by column-switching HPLC with fluorescence detection. J. Chromatogr. B Analyt. Technol. Biomed. Life Sci. *879*, 3214–3219. https://doi.org/10.1016/j.jchromb.2011.02.015.

20. Hasegawa, H., Fukushima, T., Lee, J.-A., Tsukamoto, K., Moriya, K., Ono, Y., and Imai, K. (2003). Determination of serum D-lactic and L-lactic acids in normal subjects and diabetic patients by column-switching HPLC with pre-column fluorescence derivatization. Anal. Bioanal. Chem. *377*, 886–891. https://doi.org/10.1007/s00216-003-2108-6.

21. Zhang, R., Chen, Y.N., Zhang, J., and Liu, J. (2023). Elevated serum levels of diamine oxidase, D-lactate and lipopolysaccharides are associated with metabolic-associated fatty liver disease. Eur. J. Gastroenterol. Hepatol. *35*, 94–101. https://doi.org/10.1097/MEG.0000000000002456.

22. Yan, Y., Xu, R., Li, X., Yao, Z., Zhang, H., Li, H., and Chen, W. (2022). Unexpected immunoregulation effects of D-lactate, different from L-lactate. Food Agric. Immunol. *33*, 286–301. https://doi.org/10.1080/09540105.2022.2068508.

23. Zucoloto, A.Z., Schlechte, J., Ignacio, A., Thomson, C.A., Pyke, S., Yu, I.-L., Geuking, M.B., McCoy, K.D., Yipp, B.G., Gillrie, M.R., et al. (2023). Vascular traffic control of neutrophil recruitment to the liver by microbiota-endothelium crosstalk. Cell Rep. *42*, 112507. https://doi.org/10.1016/j.celrep.2023.112507.

24. McDonald, B., Zucoloto, A.Z., Yu, I.-L., Burkhard, R., Brown, K., Geuking, M.B., and McCoy, K.D. (2020). Programing of an Intravascular Immune Firewall by the Gut Microbiota Protects against Pathogen Dissemination during Infection. Cell Host Microbe *28*, 660–668.e4. https://doi.org/10.1016/j.chom.2020.07.014.

25. Lund, J., Breum, A.W., Gil, C., Falk, S., Sass, F., Isidor, M.S., Dmytriyeva, O., Ranea-Robles, P., Mathiesen, C.V., Basse, A.L., et al. (2023). The anorectic and thermogenic effects of pharmacological lactate in male mice are confounded by treatment osmolarity and co-administered counterions. Nat. Metab. *5*, 677–698. https://doi.org/10.1038/s42255-023-00780-4.

26. Goldberg, J.S. (2011). Stereocomplexes Formed From Select Oligomers of Polymer d-lactic Acid (PDLA) and l-lactate May Inhibit Growth of Cancer Cells and Help Diagnose Aggressive Cancers-Applications of the Warburg Effect. Perspect. Medicin. Chem. *5*, 1–10. https://doi.org/10.4137/PMC.S6229.

27. Lasprilla, A.J.R., Martinez, G.A.R., Lunelli, B.H., Jardini, A.L., and Filho, R. M. (2012). Poly-lactic acid synthesis for application in biomedical devices — A review. Biotechnol. Adv. *30*, 321–328. https://doi.org/10.1016/j.biotechadv.2011.06.019.

28. Desjardins, E.M., Wu, J., Lavoie, D.C.T., Ahmadi, E., Townsend, L.K., Morrow, M.R., Wang, D., Tsakiridis, E.E., Batchuluun, B., Fayyazi, R., et al. (2023). Combination of an ACLY inhibitor with a GLP-1R agonist exerts additive benefits on nonalcoholic steatohepatitis and hepatic fibrosis in mice. Cell Rep. Med. *4*, 101193. https://doi.org/10.1016/j.xcrm.2023.101193.

29. Soffer, L.J. (1937). METABOLISM OF SODIUM d-LACTATE: I. UTILIZATION OF INTRAVENOUSLY INJECTED SODIUM d-LACTATE BY NORMAL PERSONS. Arch. Intern. Med. (Chic) *60*, 876. https://doi.org/10.1001/archinte.1937.00180050143010.

30. Ling, B., Peng, F., Alcorn, J., Lohmann, K., Bandy, B., and Zello, G.A. (2012). D-Lactate altered mitochondrial energy production in rat brain and heart but not liver. Nutr. Metab. (Lond.) *9*, 6. https://doi.org/10.1186/1743-7075-9-6.

31. Jin, S., Chen, X., Yang, J., and Ding, J. (2023). Lactate dehydrogenase D is a general dehydrogenase for D-2-hydroxyacids and is associated with D-lactic acidosis. Nat. Commun. *14*, 6638. https://doi.org/10.1038/s41467-023-42456-3.

32. Brooks, G.A. (2018). The Science and Translation of Lactate Shuttle Theory. Cell Metab. *27*, 757–785. https://doi.org/10.1016/j.cmet.2018.03.008.

33. Yao, Z., Chen, J., Li, X., Liang, S., Zhang, H., Li, H., and Chen, W. (2024). Dietary D-lactate intake ameliorates metabolic syndrome via enhancing brown adipose tissue thermogenesis in diet-induced obese mice. Food Biosci. *62*, 105284. https://doi.org/10.1016/j.fbio.2024.105284.

34. Liu, C., Wu, J., Zhu, J., Kuei, C., Yu, J., Shelton, J., Sutton, S.W., Li, X., Yun, S.J., Mirzadegan, T., et al. (2009). Lactate Inhibits Lipolysis in Fat Cells through Activation of an Orphan G-protein-coupled Receptor, GPR81. J. Biol. Chem. *284*, 2811–2822. https://doi.org/10.1074/jbc.M806409200.

35. Peiseler, M., Schwabe, R., Hampe, J., Kubes, P., Heikenwälder, M., and Tacke, F. (2022). Immune mechanisms linking metabolic injury to inflammation and fibrosis in fatty liver disease – novel insights into cellular communication circuits. J. Hepatol. *77*, 1136–1160. https://doi.org/10.1016/j.jhep.2022.06.012.

36. Chen, J., Liang, B., Bian, D., Luo, Y., Yang, J., Li, Z., Zhuang, Z., Zang, S., and Shi, J. (2019). Knockout of neutrophil elastase protects against western diet induced nonalcoholic steatohepatitis in mice by regulating hepatic ceramides metabolism. Biochem. Biophys. Res. Commun. *518*, 691–697. https://doi.org/10.1016/j.bbrc.2019.08.111.

37. Pulli, B., Ali, M., Iwamoto, Y., Zeller, M.W.G., Schob, S., Linnoila, J.J., and Chen, J.W. (2015). Myeloperoxidase–Hepatocyte–Stellate Cell Cross Talk Promotes Hepatocyte Injury and Fibrosis in Experimental Nonalcoholic Steatohepatitis. Antioxid. Redox Signal. *23*, 1255–1269. https://doi.org/10.1089/ars.2014.6108.

38. Negrin, K.A., Roth Flach, R.J., DiStefano, M.T., Matevossian, A., Friedline, R.H., Jung, D., Kim, J.K., and Czech, M.P. (2014). IL-1 Signaling in Obesity-Induced Hepatic Lipogenesis and Steatosis. PLoS One *9*, e107265. https://doi.org/10.1371/journal.pone.0107265.

39. Li, H., Zhou, Y., Wang, H., Zhang, M., Qiu, P., Zhang, M., Zhang, R., Zhao, Q., and Liu, J. (2020). Crosstalk Between Liver Macrophages and Surrounding Cells in Nonalcoholic Steatohepatitis. Front. Immunol. *11*, 1169. https://doi.org/10.3389/fimmu.2020.01169.

40. Schertzer, J.D., Tamrakar, A.K., Magalhães, J.G., Pereira, S., Bilan, P.J., Fullerton, M.D., Liu, Z., Steinberg, G.R., Giacca, A., Philpott, D.J., et al. (2011). NOD1 activators link innate immunity to insulin resistance. Diabetes *60*, 2206–2215. https://doi.org/10.2337/db11-0004.

41. Frégeau-Proulx, L., Lacouture, A., Berthiaume, L., Weidmann, C., Harvey, M., Gonthier, K., Pelletier, J.-F., Neveu, B., Jobin, C., Bastien, D., et al. (2022). Multiple metabolic pathways fuel the truncated tricarboxylic acid cycle of the prostate to sustain constant citrate production and secretion. Mol. Metab. *62*, 101516. https://doi.org/10.1016/j.molmet.2022.101516.

42. Lacouture, A., Jobin, C., Weidmann, C., Berthiaume, L., Bastien, D., Laverdière, I., Pelletier, M., and Audet-Walsh, É. (2021). A FACS-Free Purification Method to Study Estrogen Signaling, Organoid Formation, and Metabolic Reprogramming in Mammary Epithelial Cells. Front. Endocrinol. (Lausanne) *12*, 672466. https://doi.org/10.3389/fendo.2021.672466.

43. Fiehn, O. (2016). Metabolomics by Gas Chromatography-Mass Spectrometry: Combined Targeted and Untargeted Profiling. Curr. Protoc. Mol. Biol. *114*, 30.4.1–30.4.32. https://doi.org/10.1002/0471142727.mb3004s114.

44. Patel, D.P., Krausz, K.W., Xie, C., Beyoğlu, D., Gonzalez, F.J., and Idle, J. R. (2017). Metabolic profiling by gas chromatography-mass spectrometry

of energy metabolism in high-fat diet-fed obese mice. PLoS One *12*, e0177953. https://doi.org/10.1371/journal.pone.0177953.

45. Mohammadi, F., Green, M., Tolsdorf, E., Greffard, K., Leclercq, M., Bilodeau, J.-F., Droit, A., Foster, J., Bertrand, N., and Rudkowska, I. (2023). Industrial and Ruminant Trans-Fatty Acids-Enriched Diets Differentially Modulate the Microbiome and Fecal Metabolites in C57BL/6 Mice. Nutrients *15*, 1433. https://doi.org/10.3390/nu15061433.

46. Samson, N., Bosoi, C.R., Roy, C., Turcotte, L., Tribouillard, L., Mouchiroud, M., Berthiaume, L., Trottier, J., Silva, H.C.G., Guerbette, T., et al. (2024). HSDL2 links nutritional cues to bile acid and cholesterol homeostasis. Sci. Adv. *10*, eadk9681. https://doi.org/10.1126/sciadv.adk9681.

47. Daniel, N., Nachbar, R.T., Tran, T.T.T., Ouellette, A., Varin, T.V., Cotillard, A., Quinquis, L., Gagné, A., St-Pierre, P., Trottier, J., et al. (2022). Gut microbiota and fermentation-derived branched chain hydroxy acids mediate health benefits of yogurt consumption in obese mice. Nat. Commun. *13*, 1343. https://doi.org/10.1038/s41467-022-29005-0.

48. Strath, M., Warren, D.J., and Sanderson, C.J. (1985). Detection of eosinophils using an eosinophil peroxidase assay. Its use as an assay for eosinophil differentiation factors. J. Immunol. Methods *83*, 209–215. https://doi.org/10.1016/0022-1759(85)90242-X.

49. Yu, H.-P., Yang, S., Hsieh, Y.-C., Choudhry, M.A., Bland, K.I., and Chaudry, I.H. (2006). Maintenance of lung myeloperoxidase activity in proestrus females after trauma-hemorrhage: upregulation of heme oxygenase-1. Am. J. Physiol. Lung Cell. Mol. Physiol. *291*, L400–L406. https://doi.org/10.1152/ajplung.00537.2005.

50. Cissell, D.D., Link, J.M., Hu, J.C., and Athanasiou, K.A. (2017). A Modified Hydroxyproline Assay Based on Hydrochloric Acid in Ehrlich's Solution Accurately Measures Tissue Collagen Content. Tissue Eng. Part C Methods *23*, 243–250. https://doi.org/10.1089/ten.tec.2017.0018.

51. Rodrigues E-Lacerda, R., Barra, N.G., Fang, H., Anhê, G.F., and Schertzer, J.D. (2024). NOD2 protects against allergic lung inflammation in obese female mice. iScience *27*, 111130. https://doi.org/10.1016/j.isci.2024.111130.

Please cite this article in press as: Fang et al., Gut substrate trap of D-lactate from microbiota improves blood glucose and fatty liver disease in obese mice, Cell Metabolism (2025), https://doi.org/10.1016/j.cmet.2025.07.001

CellPress
OPEN ACCESS

STAR★METHODS

KEY RESOURCES TABLE

REAGENT or RESOURCE	SOURCE	IDENTIFIER
Chemicals and Reagents		
Sodium L-lactate	Sigma Aldrich	L7022
Sodium D-lactate	Sigma Aldrich	71716
[3-^{13}C] sodium D-lactate	Cambridge Isotope Laboratories	CLM-10768-PK
[3-^{13}C] sodium L-lactate	Cambridge Isotope Laboratories	CLM-1579-0.1
[C^{14}] D-lactate	American Radiolabeled Chemicals	ARC-0593-50
[C^{14}] L-lactate	American Radiolabeled Chemicals	ARC 3081-50
Collagenase from *Clostridium histolyticum* type IV	Sigma Aldrich	C5138
EGTA	BioShop	EGT202.50
HEPES	Sigma/BioShop	H3375/HEP001
William's E medium	Wisent	301-018-CL
Dulbecco's Modification Eagle's Medium (DMEM) without glucose/phenol red/L-Glutamine/Sodium Pyruvate	gibco	A14430-01
Fetal Bovine Serum (FBS)	Wisent	098-150
Phosphate Buffered Saline (PBS)	Wisent	311-010-CL
Antibiotic-antimycotic mixture	Wisent	450115EL
L-glutamine	Invitrogen	25031049
D-glucose	Sigma Aldrich	G7021-1KG
Sodium pyruvate	Sigma Aldrich	P2256-5G
NovoRapid® (Insulin)	Novo Nordisk Canada	DIN02244353
o-Dianisidine dihydrochloride	Sigma Aldrich	D3252-5G
o-Phenylenediamine 98%	Beantown Chemical	H2116750-25G
Hydrogen peroxide	EMD	HX0635
Potassium Phosphate Dibasic	Sigma Aldrich	P3786-500G
Sulfuric Acid	EM Science	7664-93-9
Hydrochloric Acid	Sigma Aldrich	258148–2.5L
Sodium Hydroxide	Sigma Aldrich	221465-500G
Isopropanol	VWR BDH Chemicals	BDH1133-1LP
Bovine collagen type I	Sigma Aldrich	C9879-1G
Chloramine T Trihydrate	Sigma Aldrich	402869-100G
4-(Dimethylamino)benzaldehyde (MDAB)	Sigma Aldrich	156477-25G
Hexadecyltrimethylammonium bromide (CTAB)	Bio Basic Inc.	CB0108
Acetic acid Glacial	Caledon Laboratories Inc.	1000-1-29
Citric acid	Caledon Laboratories Inc.	3020–1
Sodium acetate	Sigma Aldrich	S2889
Sodium citrate, dihydrate	BioShop	CIT001
Tween20	Sigma Aldrich	P1379
Hematoxylin	Sigma Aldrich	GHS232
Ammonium hydroxide solution	Sigma Aldrich	320145
Lithium carbonate, ACS, for MI	Sigma Aldrich	62470
Lactobacillus MRS Broth w/o Dextrose	Cepham Life Sciences	66416-0
Ampicillin trihydrate	Sigma Aldrich	A6140

(*Continued on next page*)

Please cite this article in press as: Fang et al., Gut substrate trap of D-lactate from microbiota improves blood glucose and fatty liver disease in obese mice, Cell Metabolism (2025), https://doi.org/10.1016/j.cmet.2025.07.001

Continued

REAGENT or RESOURCE	SOURCE	IDENTIFIER
Neomycin trisulfate salt hydrate	Sigma Aldrich	N6836
Ultrapure LPS from *E. coli* (O111:B4)	InvivoGen	TLRL-3PELPS
D-Glucose (1-^{13}C, 98-99%)	Cambridge Isotope Laboratories Inc.	CLM-420-0.25
Lactulose (U-$^{13}C_{12}$, 99%)	Cambridge Isotope Laboratories Inc.	CLM-9043-PK
[1-$^{13}C^{fru}$] lactulose	Omicron	LAC-009
Dulbecco's Modification Eagle's Medium (DMEM) with 4.5 g/L glucose and 2 mM l-glutamine	Wisent	319-051
Penstrep	Wisent	450–201
Normocin	InvivoGen	ANT-NR-05
HEK Blue detection media	InvivoGen	HB-DET2
HEK Blue selection media	InvivoGen	HB-SEL
PURASORB PL10	Corbion	N/A
PURASORB PL38	Corbion	N/A
PURASORB PL65	Corbion	N/A
PURASORB PL24	Corbion	N/A
PURASORB PD24	Corbion	N/A
PURASORB PDL20	Corbion	N/A
Critical commercial assays		
Pierce™ BCA Protein Assay Kit	Thermo Scientific	23225
Amplite™ Colorimetric D-Lactate Dehydrogenase (LDH) Assay Kit	AAT Bioquest	13809
Amplite® Colorimetric L-Lactate Dehydrogenase (LDH) Assay Kit	AAT Bioquest	13813
PicoProbe D-Lactate Assay Kit (Fluorometric)	Abcam	ab174096
Picoprobe L-Lactate Assay Kit (Fluorometric)	Abcam	ab169557
Amplite™ Fluorimetric D-Lactate Assay Kit	AAT Bioquest	13810
Amplite® Fluorimetric L-Lactate Assay Kit	AAT Bioquest	13814
Glycogen Assay Kit II (Colorimetric)	Abcam	ab169558
Triglyceride Assay Kit	Abcam	ab65336
High sensitive mouse insulin immunoassay kit	ImmunoDiagnostics	32270
VECTASTAIN Elite ABC-HRP Kit, Rabbit IgG	BioLynx	VECTPK6101
Antibodies		
F4/80 (D2S9R) XP Rabbit mAb	Cell Signaling Technology	Cat# 70076T; RRID: AB_2799771
α-smooth muscle actin (D4K9N) XP Rabbit mAb	Cell Signaling Technology	Cat# 19245T; RRID: AB_2857972
Experimental Models: Organisms/Strains		
Mouse: C57BL/6N	Taconic Biosciences, Inc.	RRID:IMSR_TAC:B6
Mouse: C57BL/6N Germ-free	In-house colonies bred in the Farncombe Gnotobiotic Unit at the McMaster Animal Facilities	N/A
Mouse: Ob/Ob$^{-/-}$	The Jackson Laboratory	RRID:IMSR_JAX:000632
Mouse: C57BL/6J	The Jackson Laboratory	RRID:IMSR_JAX:000664
Lactobacillus reuteri I49	Gifted by Dr. Kathy McCoy (UCalgary)	N/A
Lactobacillus intestinalis ASF360	Gifted by Dr. Kathy McCoy (UCalgary)	N/A
Lactobacillus delbrueckii subsp. bulgaricus	ATCC	11842
HEK-293T mTLR4 Cells	InvivoGen	HKB-mTLR4

(*Continued on next page*)

Please cite this article in press as: Fang et al., Gut substrate trap of D-lactate from microbiota improves blood glucose and fatty liver disease in obese mice, Cell Metabolism (2025), https://doi.org/10.1016/j.cmet.2025.07.001

CellPress
OPEN ACCESS

Continued

REAGENT or RESOURCE	SOURCE	IDENTIFIER
Rodent Diets		
60% HFD	Research Diets	D12492
60% HFD + 10% PL24	Research Diets	Diet formula in Table S1
60% HFD + 10% PL10	Research Diets	Diet formula in Table S1
60% HFD + 10% PL38	Research Diets	Diet formula in Table S1
60% HFD + 10% PL65	Research Diets	Diet formula in Table S2
60% HFD + 2% PL65	Research Diets	Diet formula in Table S2
60% HFD + 5% PL65	Research Diets	Diet formula in Table S2
60% HFD + 20% PL65	Research Diets	Diet formula in Table S2
Control diet	Research Diets	D09100304
MASH diet	Research Diets	D19101102
MASH diet + 20% PL65	Research Diets	Diet formula in Table S1
Software		
GraphPad Prism Version 10	GraphPad Software	RRID:SCR_002798
Qupath Version 0.5.1	Qupath	RRID:SCR_018257
ImageJ2 Version 2.14.0/1.53v	NIH	RRID:SCR_002285

EXPERIMENTAL MODEL AND SUBJECT DETAILS

Human samples

Human plasma samples were obtained from an existing biobank and ongoing experiment in humans at Université Laval. Patients with obesity were bariatric surgery candidates (average BMI = 43.14 kg/m^2 ± 0.48) with at least one metabolic syndrome, including type 2 diabetes, hypertension, or dyslipidemia. Non-obese people (average BMI = 26.76 kg/m^2 ± 0.33) were participants without obesity from the control group of an ongoing, prospective, and observational study on bone outcomes. Inclusion criteria included: adult male or female; BMI in the overweight category (25.0 to 29.9 kg/m2); not meeting the Diabetes Canada criteria for diabetes or pre-diabetes (HbA1c <6.0% and fasting blood glucose <6.1 mmol/L). All participants provided written, informed consent, and the study was approved by the Quebec Heart and Lung Institute Research Centre Ethics Review Board (MP-10-2018-2957, 2015-2466, 21160 and 2016-2569, 21237).

Animal models

All animal experiments were done in accordance with the Canadian Council on Animal Care and approved by the Animal Review Ethics Board (AREB) at McMaster University and the Animal Care Committee at the University of Ottawa, with approved Animal Use Protocols. C57BL/6J and *ob/ob* mice were purchased from the Jackson Laboratory (Bar Harbor, ME, USA). C57BL/6N mice were purchased from Taconic Biosciences (Germantown, NY, USA). C57BL/6N germ-free mice were bred in the Farncombe Gnotobiotic Unit at the McMaster Central Animal Facility. During experiments, all mice were housed in a specific pathogen-free room maintained at 22-23°C and on a 12 h light/dark cycle with free access to food and water. Mice in the MAFLD/MASH study were housed at 29-30°C during the experiment.

METHOD DETAILS

Biochemical analysis

Plasma insulin was assessed using high-sensitive mouse insulin immunoassay kit (ImmunoDiagnostics, Cat# 32270). D-lactate was determined using PicoProbe D-Lactate Assay Kit (Fluorometric) (abcam, Cat# ab174096) or Amplite™ Fluorimetric D-Lactate Assay Kit (AAT Bioquest, Cat#13810). L-lactate was determined using PicoProbe L-Lactate Assay Kit (Fluorometric) (abcam, Cat# ab169557) or Amplite® Fluorimetric L-Lactate Assay Kit (AAT Bioquest, Cat#13814). D-LDH and L-LDH enzyme activity was measured using Amplite™ Colorimetric D-Lactate Dehydrogenase (LDH) Assay Kit (AAT Bioquest, Cat# 13809) and Amplite® Colorimetric L-Lactate Dehydrogenase (LDH) Assay Kit (AAT Bioquest, Cat# 13813), respectively. Liver glycogen and triglyceride were determined using Glycogen Assay Kit II (Colorimetric) (abcam, Cat# ab169558) and Triglyceride Assay Kit (abcam, Cat# ab65336), respectively.

D- and L-lactate levels during obesity

Adult male WT (C57BL/6J) and ob/ob mice were 10 and 20 weeks old when they were fasted for 4 hours and refed for 2 hours before portal and cardiac blood were collected, and serum was isolated. Mice were sacrificed and the liver was collected and flash-frozen in liquid nitrogen. In a separated cohort of WT and *ob/ob* mice at 10 weeks old, half of the ob/ob mice were place on a broad spectrum of

antibiotics (1.0 g/L ampicillin and 0.5 g/L neomycin in the drinking water, changed every 2 days) for one week, blood glucose was monitored every two days. Mice were sacrificed and cardiac blood, cecum and feces were collected and flash-frozen in liquid nitrogen. All samples were stored at -80°C until further analysis.

Circulating D- and L-lactate levels during lactate tolerance tests

Chow and HFD-fed mice were fasted for 12 h before the test. Tail blood samples were collected at time 0, 30, 90 min after injecting 4 g/kg or gavaging 1 g/kg of sodium D- and L-lactate. In a separate cohort of chow and HFD-fed mice, portal blood samples were collected at time 0, 10, 20 min after gavaging 1 g/kg of sodium D-lactate.

D- and L-lactate in germ-free and conventionalized mice

Conventionalized male mice were obtained by exporting germ-free mice from the axenic gnotobiotic unit and mixing the dirty bedding from SPF mice with that of previously germ-free mice weekly for 23 weeks. Blood from the portal vein of age-matched germ-free and conventionalized mice was collected after 24 h fasting or in a random-fed condition.

Liver glycogen and triglyceride in germ-free and SPF mice after D- and L-lactate injection

Germ-free and SPF mice were sacrificed after 12 h fasting or after 12 h fasting and 2 h refeeding. After 12 h fasting and 12 h fasting and 2 hours refeeding, mice were injected (4g/kg, i.p.) with sodium L-lactate or equimolar sodium D-lactate. All mice were sacrificed 2 hours after the injection. Livers were excised and flash-frozen in liquid nitrogen. All samples were stored at -80°C until further analysis.

Glucose and lactate tolerance tests

Mice were 6 h-fasted and tail blood glucose was measured after injection of glucose (0.7 g/kg i.p.) using a glucometer (StatStrip Xpress®, Nova Biomedical). C57BL/6N mice were kept on either a control diet or 60% HFD (Research Diets, D12492) for 8 weeks. After 12 h fasting, these mice were gavaged with 1g/kg of sodium L-lactate or D-lactate and blood glucose was measured using a glucometer. The area under the curve (AUC) was calculated using GraphPad Prism (v10).

In vivo lactate injections

Mice were fasted overnight from 7pm-7am, then re-fed for 2 h. Radiolabelled D- or L-lactate (5 μCi per mouse) was then injected via the tail vein. Following injection, ~10 μl of blood was collected from the tail every 5 mins for 30 mins. Serum was separated via centrifugation at 4 degrees at 5,000 x g and radioactivity was determined using 2 μl of serum using liquid scintillation counting. After 30 min, mice were sacrificed, and tissues were removed and stored at -80°C degrees. To determine the incorporation of D- or L-lactate in the lipid fraction, tissues were homogenized in ice-cold PBS prior to undergoing a lipid extraction (Bligh and Dyer), protein determination using BCA (Thermo Scientific), and radioactivity determination using liquid scintillation counting.

In vivo 13C tracing

A gut commensal (*Lactobacillus delbrueckii subsp. bulgaricus*) was cultured with MRS broth (without dextrose). [1-$^{13}C^{fru}$] lactulose was added to the MRS broth to trace the production of D-lactate from lactulose. The metabolites in the bacteria culture media were extracted using methanol and acetonitrile. D- and L-lactate was analyzed using a chiral column via LC/MS. For ^{13}C tracing in mice, germ-free and SPF mice were housed in Promethion Metabolic Cages (Sable Systems International, USA). A ^{13}C-labeled tracer was gavaged into each mouse and ^{13}C in the CO_2 from their breath was measured using the stable isotope gas analyzer.

Mouse primary hepatocytes

Male C57BL/6N mice were fasted for 12 hours and refed for 3 hours and primary hepatocytes were isolated, as described.[40] Then glucose (10 mM), pyruvate (1 mM), insulin (100 nM), and lactate (10 mM, non-labeled and ^{13}C-labeled D- and L-lactate) were added to each well, and 8 h later cells were rinsed with ice-cold saline (NaCl 0.9%) and harvested in dry-ice cold 80% MeOH. In a separate mouse primary hepatocyte isolation, physiological doses of D-lactate and L-lactate were used to treat the cells. The treatment conditions were glucose (10 mM), insulin (100 nM), D-Lactate (0.4 mM, non-labeled and ^{13}C-labeled), L-lactate (4 mM, non-labeled and ^{13}C-labeled). Pyruvate was added in 1:10 ratio to lactate concentration in each well. Cell extracts were then kept at -80°C until further analysis. For metabolomics with Gas Chromatography-Mass Spectrometry (GC-MS) cell extracts were analyzed by targeted metabolomics, as previously described,[41,42] using an Agilent 8890 GC equipped with a DB5-MS+DG capillary column coupled to an Agilent 5977B MS instrument.

Mouse primary hepatocytes metabolite quantification

To quantify TCA cycle intermediates, D-lactate or L-lactate, and palmitate, myristic acid-d27 was added as an internal standard to the samples. Cells were then lysed by sonication before centrifugation (10 min at 20,000 g). Supernatants were harvested, transferred to a new tube containing 700 μL of acetonitrile (ACN), vortexed, and centrifuged. For the quantification of glucose and pyruvate, small modifications to the protocol described above were performed. Myristic acid d-27 and xylose were added as internal standards to the samples. Samples were then lysed by sonication; they were then centrifuged, and supernatants were harvested and kept at 4°C. The pellet obtained was rinsed with purified water, vortexed, and centrifuged. The water supernatant was added to the first supernatant and centrifuged (10 min at 20,000 g). For both methods, the resulting supernatants were dried using nitrogen gas before a

2-step derivatization protocol. First, methoxyamination was performed using the protocol by Fiehn et al.[43] Second, we performed silylation with MTBSTFA/1%TBDMCS using the modified protocol from Patel and coworkers for the first analysis method.[44] For glucose and pyruvate, we performed silylation with MSTFA/1% TCMS using the protocol by Fiehn et al.[43] Then, samples were injected into the GC-MS system (1 μL was injected in split mode at 250°C). The carrier gas, helium, was kept at a constant flow rate of 1mL/min. The GC oven temperature oven was held at 50°C for 2 min, then raised to 150°C at a rate of 20°C/min for 5 min, and from 150°C to 300°C at a rate of 10°C/ min; column temperature was then kept constant at 300°C for another 10 min. The quadrupole was held at 150°C and the MS source at 230°C. The scanning mode for a mass range of 50 to 650 Da. The Agilent MassHunter Workstation Software was used to perform analyses and metabolites were identified with the NIST/EPA/NIH Mass Spectral Library (NIST 2017, Gaithersburg, MD, USA). Metabolite levels were normalized with the internal standard(s) and for cell number. Isotopomer quantification was further corrected for their natural abundance measured in samples with L/D-Lactate.

Colonization of Germ-free mice with D-lactate producers

Lactobacillus intestinalis ASF360 (D-lactate^{HIGH}, which produces high levels of D-lactate) or *Lactobacillus reuteri 149* (D-lactate^{LOW}, which produces low levels of D-lactate) were cultured in MRS media in an anaerobic chamber at 37 °C. and CFU was determined using an MRS plate. Germ-free mice were colonized with D-lactate^{HIGH} or D-lactate^{LOW} bacteria at upon export from the axenic gnotobiotic unit (i.e., week 0) and then re-colonized on week 6 by gavaging 1 x10^9 CFU/mL of live bacteria. Body weight, food intake, and random-fed blood glucose were recorded weekly. Blood and fecal samples were collected throughout the study, where indicated.

Acute polylactide administration

Polylactide was from Corbion (Gorinchem, Netherlands) and then reduced to a fine powder using a Polymix® Laboratory Grinding Mills (PX-MFC 90 D, Kinematica, Switzerland) and stored at -20 °C. For acute experiments, powdered polymers were mixed with saline (1:1 [w:v]) to yield a uniform resuspension. SPF Mice were fasted for 24 h and subsequently fed with small increments of saline-sorbed PDL20, PD24 or PL24 (approximate final dose = 100 mg/mouse). PL24 and PD24 polymers were also tested in 24 h-fasted Germ-free mice and Germ-free mice colonized with D-lactate^{LOW} producing bacteria (two weeks after colonization). Blood glucose was monitored before (0h) and 4h after administration of different polymers. PL24 was packed into a 60% HFD and fed to a separate cohort of mice, where 35-week-old mice were on a 60% high-fat diet (HFD) for 29 weeks and then switched to 60% HFD + 10% PL24 (w:w) for 1 day. These obese mice were fasted for 18 h and then refed for 2 h with 60% HFD or 60% HFD + 10% PL24 and then mice were sacrificed, livers were excised, and triglycerides were determined.

Long-term feeding with PL24

Six-week-old male C57BL/6N mice were kept on HFD for 23 weeks and then switched to a HFD supplemented with 10% PL24 (w:w) whereas a control group was kept on the HFD for 7 additional weeks. Body weight, food intake, and random-fed blood glucose were monitored weekly. On week 4, mice were individually placed in clean cages without bedding, and feces were collected for lactate output assessment. On week 6 random fed blood D- and L-lactate were measured. On week 7, blood glucose, insulin, and D- and L-lactate were measured in mice after 12h fasting and HOMA-IR calculated (Fasting Insulin [mIU/L] x Fasting Glucose [mmol/L])/22.5). The polymer length and dose study are performed in the same animal model. Details of these studies are in supplementary.

Polylactide length and dose study

Six-week-old male C57BL/6N mice were kept on HFD for 23 weeks. Mice were then randomized into four groups: control (60% HFD only), PL10 (60% HFD + 10% PL10), PL38 (60% HFD + 10% PL38), and PL65 (60% HFD + 10% PL65). They were kept on their assigned diet for 9 weeks. Body weight, food intake and random-fed blood glucose was monitored weekly. At week 8, blood glucose and insulin were monitored after 4h fasting. HOMA-IR was used to assess fasting insulin resistance and was calculated as follows: (Fasting insulin [mIU/L] x Fasting Glucose [mmol/L])/22.5. In a separate cohort, 6-week-old male C57BL/6N mice were kept on HFD for 23 weeks. They were randomized into five groups: control (60% HFD only), PL65_2% (60% HFD + 2% PL65), PL65_5% (60% HFD + 5% PL65), PL65_10% (60% HFD + 10% PL65), and PL65_20% (60% HFD + 20% PL65) and remained on their designated diet for 4 weeks. Body weight, food intake and random-fed blood glucose was monitored weekly. At week 3, a glucose tolerance test was performed in these mice after 6h fasting. At week 4, 4h fasting blood glucose were monitored.

Fecal targeted metabolomics

For targeted metabolomics in mouse fecal samples, feces from individual mice were first crushed and homogenized on dry ice, before lyophilization. To measure short-chain fatty acids, samples were processed by the *Service d'analyse ciblée du metabolome par GC/MS* at the Centre de recherche du CHU de Québec – Université Laval. A slightly modified method of the one published by Mohammadi et al. was used.[45] In brief, 10 mg of powdered feces was mixed with 100 mg of sodium chloride, 20 μL of phosphoric acid (85%), 35 μL of milli-Q water and 8 μL of internal standard (2-ethylbutyric acid). Then, 150 μL of acetonitrile was added, followed by thorough mixing and centrifugation for 2 min at 16,000 *g*. The upper phase was harvested and, after 20 minutes of stirring at 85°C, 500 μL of the gas phase was injected into a ZB-FFAP column (Phenomenex) and analyzed on a gas chromatograph-mass spectrometer system (as detailed in[45]). Absolute quantification was performed using a calibration curve with standards. For bile acids, powdered feces samples were sent to the metabolomics platform and bioanalytical services of the Centre de recherche du CHU

de Québec – Université Laval for absolute quantification by LC-MS/MS, using the same method as previously published.[46,47] For the relative quantification of amino acids and succinate, powdered feces were resuspended in 80% methanol to obtain a 10mg/mL solution. Samples were sonicated twice for 10 min (30 sec on/off) before being centrifuged at 20,000 *g* for 10 min at 4°C. A volume of 200 μL per sample was transferred to a new tube, combined with the internal standard by vortexing, and dried using nitrogen. Finally, samples were processed as described for stable isotope tracer analysis.

PL65 in MAFLD/MASH

Twelve-week-old male C57BL/6N mice were fed a control diet (Research diets: D09100304), MASH diet (D19101102), or MASH diet containing 20% (w:w) PL65 (see Table S1). Mice were housed in Solace Zone (ARES Scientific) thermoneutral cages at 29°C for 20 weeks. Body weight, food intake and random-fed blood glucose was monitored weekly. At week 19, 4h fasting blood glucose and serum insulin were measured. Mice were sacrificed at week 20 in the random-fed state and the liver was separated into the five lobes (left lateral, left medial, right medial, right lateral and caudate lobes) and a piece of each lobe was processed for histology.

Metabolic endotoxemia measurement via HEK TLR4 reporter cell

HEK-293T cells transfected with mouse TLR4 were purchased from InvivoGen and grown and cultured and assayed according to the manufacturer's protocol. Briefly, mouse serum samples were heated at 56°C for 10 minutes before the assay. 20 μL of *E. coli* LPS standards and mouse serum samples were added to the 96-well plate. HEK-293T cells were plated in 96-well plate at density of 15,000 or 30,000 cells/well with 180 μL of HEK-blue detection media. The plate was read at an absorbance of 630 nm after 24 h incubation.

MPO and EPO enzymatic activity assays

MPO assay protocol was followed according to Yu et al., and EPO assay protocol was followed according to Sanderson et al.[48,49] A 40-50 mg piece of the left lateral lobe of the liver was chipped and homogenized in 1X PBS in a 1:10 ratio. The homogenates were centrifuged at 10,000 rpm for 10 minutes at 4 degrees, and the supernatant and fat layer were discarded. The pellet was resuspended in 1X PBS and centrifuged again at 10,000 rpm for 10 minutes at 4 degrees. The supernatant and fat layer were discarded, and the pellet was resuspended in MPO buffer and CTAB solution. The resuspended pellet was freeze-thawed three times in liquid nitrogen, and then centrifuged at 10,000 rpm for 10 minutes at 4 degrees. The supernatant was collected for the assays. For the MPO assay, 10 uL of supernatant and 200 uL of reaction mix was added per well. Reaction mix: 5 mM potassium phosphate dibasic pH 6, 0.5 mM o-dianisidine dihydrochloride, and 0.0005% hydrogen peroxide. Absorbance was read at 460 nm immediately after adding reaction mix for 30 minutes with absorbance being measured every 5 minutes. For the EPO assay, 50 uL of supernatant and 50 uL of reaction mix was added to each well. Reaction mix: 75 mM potassium phosphate dibasic pH 8, 6.6 mM hydrogen peroxide, 1.5 mM o-phenylenediamine. Plate was left for a 10-minute incubation at room temperature. The reaction is stopped with 1 mM sulfuric acid. Absorbance was read at 492 nm. A blank well of water was included in each assay.

Hydroxyproline assay

Assay protocol was followed according to Cissell et al.[50] with some modifications as described in our previous manuscript.[51] A 20 mg piece of the left lateral lobe of the liver was chipped and homogenized in 5M HCl (1 mL of HCl was added for every 80 mg of tissue). A standard was prepared of 2.7 mg bovine collagen type I in 337 uL HCl. Tissues and standard were homogenized and autoclaved for 45 minutes. Four volumes of 1M NaOH was added per one volume of 5M HCl in each tube containing the autoclaved liver homogenates. The tubes were centrifuged at 10,000 rpm for 5 minutes. The stock standard was used to make seven 1:2 serial dilutions. 50 uL of each sample/standard was added to clear bottom plate, and two 50 uL H2O blank wells were included. 100 uL of oxidation buffer was added to each well and the plate was incubating at room temperature for 5 minutes. 100 uL of Ehrlich solution was added to each well and mixed well. The plate was then incubated at 60 degrees for 45 minutes. After incubation, the plate was left to cool down at room temperature for 10 minutes. Absorbance was then measured at 570 nm. Oxidation solution: 26% v/v isopropanol, 74% v/v H2O, 0.629 M sodium hydroxide, 0.140 M citric acid (monohydrate), 0.453 M sodium acetate pH6, 0.112 acetic acid, and 0.05 M chloramine T. Ehrlich solution: 1 M MDAB, 70% v/v isopropanol, 30% v/v HCl.

Histology and immunohistochemistry

A piece of each of the 5 liver lobes from each mouse was prepared for histology and scored by a pathologist who was blinded to the experimental conditions using MASH clinical research network scoring system using hematoxylin & eosin (H&E) and picrosirius red (PSR)-stained sections in all lobes of the liver. The tissues were fixed in 4% paraformaldehyde and shaken at 4°C for 24 hours before transferring to 70% ethanol. The tissues were paraffin-embedded and sent to McMaster Immunology Research Centre Histology Core Facility for sectioning and staining with hematoxylin and eosin (H&E) and picrosirius red (PSR). The slides were scanned at the facility with a Leica Aperio Scanscope XT at 20x magnification and sent to a pathologist for MASH activity scoring. Oil red O staining was conducted on the left lateral lobe of the liver at McMaster Immunology Research Centre Histology Core Facility. Immunohistochemistry was only conducted on the left lateral lobe of the liver for all targets. Briefly, the sections were deparaffinized and hydrated. Citrate buffer (10 mM sodium citrate in 0.05% tween20) was used for antigen retrieval after which endogenous peroxidases were blocked. The primary antibody was added, and slides were left to incubate at 4°C, in the dark overnight. The secondary antibody was added the next day and slides were incubated for 30 minutes. Finally, HRP substrate solution was added, and the slides

Please cite this article in press as: Fang et al., Gut substrate trap of D-lactate from microbiota improves blood glucose and fatty liver disease in obese mice, Cell Metabolism (2025), https://doi.org/10.1016/j.cmet.2025.07.001

were incubated for 10 minutes (α-SMA) or 8 minutes (F4/80). The slides were then stained with hematoxylin and a bluing counterstain (5N ammonium hydroxide in 70% ethanol or 0.05% lithium carbonate) after which they were dehydrated and mounted. Images were taken with a Nikon Eclipse Ni microscope at 20x magnification. ImageJ and Qupath were used for image analysis.

QUANTIFICATION AND STATISTICAL ANALYSIS

Mann-Whitney U-test was used to compare two groups. One-way analysis of variance (ANOVA) followed by Tukey's multiple comparison test was used to compare more than two groups. Two-way repeated measures ANOVA with Bonferroni's post hoc test was applied to compare between groups throughout several time-points. Statistical significance was accepted at $p < 0.05$.